Computers and Chemical Engineering 213 (2026) 109750

Contents lists available at ScienceDirect

Computers and Chemical Engineering

journal homepage: www.elsevier.com/locate/cace

Optimal design of a low-carbon concrete production plant considering variable material composition and electricity prices

Ariana Y. Ojeda-Paredes [a,b], Gourisankar Sandaka [c], Günter Beuchle [c], Peter Stemmermann [c], Dieter Stapf [c], Alexander Mitsos [d,a,e], Manuel Dahmen [a,*]

[a] Forschungszentrum Jülich GmbH, Institute of Climate and Energy Systems, Energy Systems Engineering (ICE-1), Jülich 52425, Germany
[b] RWTH Aachen University, Aachen 52062, Germany
[c] Karlsruhe Institute of Technology, Institute for Technical Chemistry (ITC), Karlsruhe 76021, Germany
[d] JARA-ENERGY, Jülich 52425, Germany
[e] RWTH Aachen University, Process Systems Engineering (AVT.SVT), Aachen 52074, Germany

ARTICLE INFO

Keywords:
Integrated design and scheduling
Demand response (DR)
Recycled belite cement clinker (RC-BCC)
Concrete production
Secondary recycled materials

ABSTRACT

Recycled belite cement clinker (RC-BCC) can partially replace conventional Portland cement to produce low-carbon concrete. We determine the optimal design of a low-carbon concrete production plant and analyze its demand response potential through process scheduling under time-varying electricity prices. To this end, we formulate and optimize an integrated design and scheduling model, combining different technologies for rotary kiln heating, carbon capture and utilization (CCU), and fuel switching. Compared to concrete production from 100% Portland cement, the global warming impact (GWI) is reduced by 27–65% at a 50% RC-BCC replacement level, depending on the kiln heating technology, fuel type, and carbon intensity of the electricity mix, highlighting the strong mitigation potential of material substitution and CCU. Across the investigated temporal aggregations of electricity price time series data, flexible operation reduces electricity costs by 2.2–2.8% for the electrically-heated rotary kiln and by 13.4–18.2% for the oxyfuel-fired rotary kiln with biomass. The corresponding load shifting amounts to 3.7–5.3% and 25.0–30.6%, respectively. However, the total annualized cost (TAC) remains similar to the non-flexible process due to the additional capital investment requirements. The results show that RC-BCC is a promising technology for greenhouse gas (GHG) reduction and material circularity in cement production.

1. Introduction

Concrete is the most widely consumed man-made material globally (Griffiths et al., 2023). Concrete is made from a mix of cement, water, and fine and coarse aggregates. Cement is the key binder material in concrete and represents approximately 10%–15% of the total concrete mass (Griffiths et al., 2023). Among different cement types, Portland cement has been the most widely used (Barbhuiya et al., 2024). However, the production of its main component Portland cement clinker (PCC) significantly contributes to CO_2 emissions, with more than 60% attributed to limestone calcination (Schorcht et al., 2013).

Efforts to decarbonize cement production have increasingly focused on material and process innovations, including the use of alternative binders or raw materials, the use of alternative fuels, carbon capture, utilization, and storage (CCUS) technologies and process electrification (Marmier, 2023; Griffiths et al., 2023). On the material side, substituting PCC for concrete production can be a helpful measure to reduce CO_2 emissions (Ishak and Hashim, 2015). Belite-rich clinkers are an alternative with a belite content between 40%–90% (International Energy Agency (IEA), 2018). These clinkers are produced at lower temperatures, approximately 1250 to 1350°C (Sabbah and Zhutovsky, 2022; Tan et al., 2020), and as low as 1000°C in recent innovations (Hunsinger et al., 2014), compared to 1450°C for PCC. This reduction in temperature decreases both energy demand and fossil fuel-related emissions (Gartner and Sui, 2018; International Energy Agency (IEA), 2018). Furthermore, integrating secondary or recycled raw materials, such as cellular concrete waste (Schoon et al., 2013) or post-demolition autoclaved aerated concrete (pd-AAC) powder (Steins et al., 2022), not only reduces CO_2 emissions, but also reduces the consumption of virgin materials and avoids landfill disposal.

Replacing traditional fuels such as hard coal or petcoke with low-carbon alternatives, and implementing carbon capture technologies can

* Corresponding author.
E-mail address: m.dahmen@fz-juelich.de (M. Dahmen).

https://doi.org/10.1016/j.compchemeng.2026.109750
Received 12 March 2026; Received in revised form 13 May 2026; Accepted 8 June 2026
Available online 18 June 2026

significantly reduce direct CO_2 emissions. Fuels like natural gas and hydrogen have demonstrated their applicability in the cement industry, showing the potential to decrease emissions related to process heat supply (Juangsa et al., 2022; El-Emam and Gabriel, 2021; Nhuchhen et al., 2021). Carbon capture, utilization, and storage (CCUS) technologies have been studied for their implementation in conventional cement production (Hills et al., 2016; Plaza et al., 2020; Voldsund et al., 2019; Gardarsdottir et al., 2019; ECRA, 2009; International Energy Agency (IEA), 2018; Juangsa et al., 2022). These technologies address emissions from both limestone calcination and fossil fuel combustion. Captured CO_2 can be used as feedstock in mineral carbonation to enhance sustainability and contribute to circular economy (Barbhuiya et al., 2024). Mineral carbonation offers permanent CO_2 storage by converting emissions into stable solid mineralized carbonates (Baena-Moreno et al., 2019; Barbhuiya et al., 2024; Bremen et al., 2022). In addition, mineral carbonation products have been proposed as supplementary cementitious materials in blended cements, enabling reductions in the carbon footprint of cement production while maintaining economic competitiveness (Bremen et al., 2022).

Process electrification in cement and concrete production, such as the electrification of heat supply (Quevedo Parra and Romano, 2023) or calciner electrification (Varnier et al., 2025; Quevedo Parra and Romano, 2023), is considered a relevant decarbonization strategy, provided that electricity is produced from renewable energy sources (RES). However, the increasing penetration of RES into electricity grids leads to stronger fluctuations in electricity generation, resulting in stronger electricity price fluctuations. In this context, demand response (DR) is a promising approach for industrial processes to adjust their electricity consumption in response to time-varying electricity prices. The benefits and limitations of DR in industrial processes have been widely discussed in the literature (see, e.g., Paulus and Borggrefe (2011), Zhang and Grossmann (2016), Mitsos et al. (2018), Schäfer et al. (2020) and Siddiquee et al. (2021)). In addition, the economic potential of DR, particularly in terms of electricity cost savings, has been evaluated in several energy-intensive sectors, including copper (Röben et al., 2022; Germscheid et al., 2023), cement (Golmohamadi, 2022; Mossie et al., 2025), iron and steel (Castro et al., 2013), and pulp and paper (Helin et al., 2017).

Following these process and material innovations, a novel recycled belite cement clinker (RC-BCC) has been recently developed. This belite clinker is produced using construction wastes, e.g., pd-AAC or concrete waste fines, as a secondary raw material, aiming to reduce CO_2 emissions and energy consumption, while mitigating the impact of natural resource exploitation (Stemmermann et al., 2022, 2024). RC-BCC is produced at a lower kiln temperature (approx. 1000°C), compared to PCC, and the rotary kiln can be powered either with fossil fuels or electricity. The RC-BCC technology is at a technology readiness level (TRL) between 4 and 5, i.e., in the stage of basic validation (Stemmermann et al., 2024), with a pilot plant facility operating at Karlsruhe Institute of Technology (KIT) to test and optimize the process, and gather data for future scaling.

Despite the potential of RC-BCC and related innovations, practical implementation of this technology presents challenges. In contrast to PCC production, which typically relies on homogeneous and well-characterized natural raw materials, the quality and homogeneity of RC-BCC may vary when secondary raw materials (SRMs) with variable composition are used (Stemmermann et al., 2024). Furthermore, as of today, RC-BCC can only partially substitute Portland cement in concrete applications. For instance, Stemmermann et al. (2022) reported substitution levels of up to 50% at the laboratory scale and 25% at the industrial scale in autoclaved aerated concrete (AAC) production. In practice, substitution ratios are often defined by the client specifications and compliance with technical standards.

In summary, RC-BCC is a promising technology that is able to (i) reduce process CO_2 emissions, (ii) partially substitute Portland cement in concrete production, (iii) utilize recycled materials, and (iv) enable process electrification. However, the optimal design and operation of RC-BCC production systems, particularly under variable electricity prices and raw material compositions have yet to be investigated.

In this study, we formulate an optimization framework for the simultaneous design and operation of a low-carbon concrete production plant based on RC-BCC. The model follows a superstructure-based approach, similar to our previous work on Ordinary Portland cement production (Ojeda-Paredes et al., 2025), and includes various alternative technologies for kiln heating (electric or oxyfuel), heat supply (market-sourced or on-site produced hydrogen, biomass, natural gas), carbon capture via oxyfuel combustion, and mineral carbonation (gaseous or aqueous). The optimization model considers both design decisions (e.g., technology selection and sizing) and time-dependent operational decisions (e.g., mass flows, operation modes), enabling the system to adapt to time-varying electricity prices and raw material inputs. The model is implemented in our open-source energy system optimization framework COMANDO (Langiu et al., 2021) and formulated and solved as a bi-objective mixed-integer linear program (MILP) to identify trade-offs between total annualized cost and global warming impact.

The remainder of this article is organized as follows: Section 2 describes the process technologies considered in the superstructure, and the relevant assumptions and parameters. Section 3 presents the mathematical formulation and solution strategy. Section 4 presents the results and discusses the trade-offs. Finally, Section 5 provides concluding remarks.

2. System description

This section provides a detailed description of the technologies, assumptions, and parameters considered in the superstructure for the production of RC-BCC based concrete. The superstructure (see Fig. 1) includes five main process blocks: (i) recycled belite cement clinker production (Section 2.1) and the heating technologies for the rotary kiln (Section 2.2), (ii) carbon capture (Section 2.3), (iii) carbon capture and utilization (Section 2.4), (iv) concrete production (Section 2.5), and (v) energy supply (Section 2.6). Storage units, commodity prices and CO_2 certificates costs, and emission factors are discussed in Sections 2.7, 2.8 and 2.9, respectively.

2.1. Recycled belite cement clinker production

The production of recycled belite cement clinker (RC-BCC) involves a series of unit operations, and various raw materials and energy sources. The production process and assumptions presented here are based on the experimental and modeling work by Stemmermann et al. (2022, 2024).

The first task is the pre-treatment of waste concrete, which is crushed to obtain coarse and fine fractions. The coarse fraction (particles > 4 mm) may be stored or used as feedstock for producing carbonate aggregates via mineral carbonation. The fine fraction (particles < 4 mm), which is rich in SiO_2 and CaO, is utilized for RC-BCC production. Due to their typical moisture content of around 15%, the fines are dried prior to milling. The dried recycled concrete fines (rCF) are milled with limestone in a ball mill. Limestone is added to increase the calcium oxide (CaO) content and to achieve a $CaO:SiO_2$ molar ratio of 2 in the raw meal, a requirement for belite cement clinker types (Stemmermann et al., 2022). The limestone addition is determined based on the target CaO content, assuming complete calcination of $CaCO_3$. The resulting raw meal is preheated up to 300°C and fed into the kiln where the calcination and clinkerization reactions take place. Potentially, recovered heat from the rotary kiln is used for preheating. To avoid undesired carbonation of the raw meal during drying in the preheater, we consider heat recovery via an indirect gas–gas heat exchanger, in which hot kiln off-gases transfer heat to an air stream

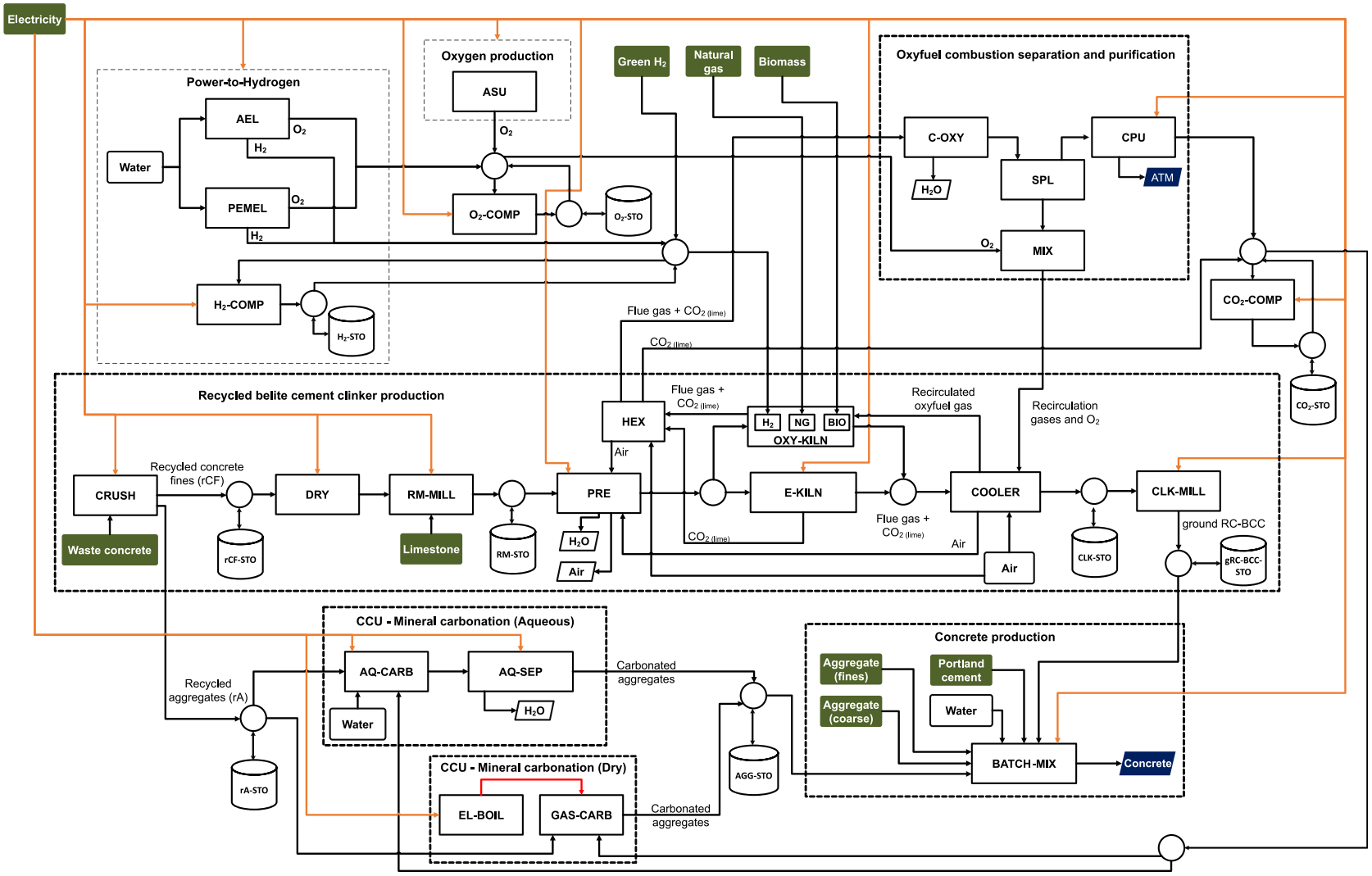

Fig. 1. Superstructure of low-carbon concrete production. The unit operations are represented by white rectangles. The storage units are represented by vertical cylinders. Electricity flows are represented by orange lines, heat flows by red lines and mass flows by black lines. Sources are represented by green rounded rectangles and sinks by blue rhombuses. Unfilled rounded rectangles and rhombuses denote auxiliary streams (air and water) included for process representation. We use the abbreviations: crusher (CRUSH), dryer (DRY), raw mill (RM-MILL), preheater (PRE), oxyfuel-fired rotary kiln (OXY-KILN), electrically-heated rotary kiln (E-KILN), clinker cooler (COOL-1), heat exchanger (HEX), clinker mill (CLK-MILL), air separation unit (ASU), alkaline electrolyzer (AEL), polymer exchange membrane electrolyzer (PEMEL), H_2 compressor (H_2-COMP), O_2 compressor (O_2-COMP), condenser for oxyfuel (C-OXY), carbon purification unit (CPU), splitter (SPL), mixer (MIX), CO_2 compressor (CO_2-COMP), aqueous mineral carbonator (AQ-CARB), filtration and drying section (AQ-SEP), electric boiler (EL-BOIL), reactor for gas–solid mineral carbonation (GAS-CARB), batching and mixing section (BATCH-MIX), recycled concrete fines storage (rCF-STO), recycled aggregates storage (rA-STO), raw meal storage (RM-STO), aggregates storage (AGG-STO), clinker storage (CLK-STO), ground recycled belite cement clinker storage (rRC-BCC-STO), hydrogen storage (H_2-STO), oxygen storage (O_2-STO), carbon dioxide storage (CO_2-STO), recycled belite cement clinker (RC-BCC), ground recycled belite cement clinker (gRC-BCC) and CO_2 emissions to atmosphere (ATM)

Table 1
RC-BCC production parameters.

Process parameters	Value	Unit
Waste concrete moisture	15	%
Limestone moisture	2	%
Preheating temperature	300	°C
Rotary kiln temperature	1000	°C

Table 2
Power consumption in RC-BCC production.

Unit	Value	Unit	Reference
Crusher	2.17	$kWh/t_{conc\text{-}waste}$	[a]
Dryer	627.7	kWh/t_{water}	Based on latent heat for water evaporation
Raw mill	19	$kWh/t_{raw\text{-}meal}$	Representative value, based on[b]
Electric kiln	538.1	$kWh/t_{belite\text{-}clinker}$	[c]
RC-BCC mill	36.5	$kWh/t_{RC\text{-}BCC}$	Representative value, based on[d]

[a] Deolalkar (2009).
[b] Atmaca and Atmaca (2016) and Meng et al. (2021).
[c] Stemmermann et al. (2024).
[d] Bhatnagar and Popuri (2024) and Genç (2016).

supplied at ambient temperature and used for preheating. The availability of recovered heat depends on the specific heating technology of the rotary kiln. In the case of the oxyfuel-fired rotary kiln, the amount of flue gas is generally sufficient to preheat the raw meal. In contrast, for the electrically-heated rotary kiln, the availability of recoverable waste heat is limited due to the absence of combustion and associated high-temperature flue gas streams. In this configuration, only CO_2 from limestone calcination is released, resulting in comparatively small gas flows. Nevertheless, part of the thermal energy can still be recovered from the hot clinker via the clinker cooler (through heated cooling air). Overall, the heat recovery potential remains lower than in the oxyfuel-fired rotary kiln configuration. For this reason, we assume electric preheating since direct electric heating systems are already established in the industry and suitable for moderate temperatures (Fraunhofer ISI, 2024). During calcination, CO_2 is released from the decomposition of limestone, while in clinkerization, belite phases are formed. To promote belite clinker formation at reduced temperatures (1000°C), a CO_2-rich atmosphere in the kiln is required (Stemmermann et al., 2022). The lower temperature compared to conventional clinker production (both belite and Portland) simplifies the integration of alternative heating technologies, such as electric heating and oxyfuel combustion, which are detailed in Section 2.2. Afterwards, the belite clinker is cooled and then ground in a ball mill to achieve the required cement fineness, resulting in the final RC-BCC product.

As no industrial RC-BCC plant currently exists, the material and energy balances used in this work are derived from laboratory tests and theoretical estimates, which are summarized in Tables 1 and 2. For the grinding steps, we use representative power-consumption values based on literature data and industrial practice (see Table 2). In particular, for raw meal grinding, Meng et al. (2021) report typical ranges of 12–22 kWh/t for roller-press final grinding, 13–17 kWh/t for external-circulation vertical mills, and 20–24 kWh/t for middle-unloading drying tube mills. Likewise, Atmaca and Atmaca (2016) report 25.52 kWh/t farine for an industrial raw mill. The value of 19 kWh/t adopted in Table 2 therefore lies within the reported industrial range and is used as a representative value for raw meal grinding in this study. For RC-BCC grinding, no direct measurements for belite clinker grinding are available in the open literature. Therefore, we adopt a value of 36.5 kWh/t as a representative value based on reported values for ball-mill cement clinker grinding. For example, Genç (2016) reports 34.2 kWh/t for a conventional multi-compartment closed-circuit ball-mill system, while Bhatnagar and Popuri (2024) report 36–37 kWh/t for closed-circuit ball-mill grinding of white cement.

In contrast to PCC, which is typically manufactured at large-scale facilities located near limestone quarries to reduce raw material transport costs (Marsh et al., 2022; Kendall et al., 2010), the viability of RC-BCC production depends on the local availability of secondary materials, i.e., waste concrete from demolition. Since regions with high volumes of demolition material are limited to metropolitan areas and availability may vary over the year, decentralized RC-BCC plants may offer logistical and environmental advantages by minimizing long-distance transport of secondary materials. Recent industry trends show that cement producers are increasingly integrating concrete recycling into their value chains, supporting the practical relevance of decentralized RC-BCC concepts (CemNet, 2025).

In this work, we assume a decentralized plant with a nominal capacity of 50 kt/a, operating 300 days annually. This capacity is based on our own order-of-magnitude estimate of the amount of demolition-derived concrete that could be supplied within urban regions.

2.2. Heating technologies for rotary kiln

Innovative heating technologies have been investigated to reduce CO_2 emissions from industrial kilns and furnaces, including oxyfuel combustion and electric heating (Pisciotta et al., 2022). In particular, for recycled belite cement clinker (RC-BCC) production, Stemmermann et al. (2024) assessed two heating technologies for the rotary kiln: oxyfuel combustion, and electric heating. Accordingly, in the present work we focus on oxyfuel-fired and electrically-heated rotary kilns, as they represent innovative low-carbon configurations that either eliminate combustion-related emissions (electrically-heated rotary kiln) or enable efficient CO_2 capture via a concentrated flue gas stream (oxyfuel-fired rotary kiln).

2.2.1. Electric rotary kiln

Electrification in the cement industry aims to replace fossil fuels in high-temperature processes in order to reduce direct CO_2 emissions. Calcination and clinkerization typically require process temperatures up to 900°C and 1450°C, respectively (Madeddu et al., 2020; Varnier et al., 2025). A range of electric heating technologies has been investigated for such applications, including plasma, induction, resistance, and microwave heating (Varnier et al., 2025; Lechtenböhmer et al., 2016; Material Economics, 2019).

Technologies such as plasma or microwave heating, which are capable of reaching extremely high temperatures, are more suited for full clinkerization processes targeting alite formation. However, for the production of belite-rich clinker at moderate temperatures (1000°C), resistance heating is more suitable. Resistance-based electric calciners have been demonstrated at pilot scale and are considered technically feasible for cement applications (Tokheim et al., 2019; LEILAC2 Project, 2023; Tsupari et al., 2022; CLIMIT Programme, 2020). Notably, the Low Emissions Intensity Lime and Cement (LEILAC) project developed a technology in which the raw meal is calcined by heat indirectly transferred from the hot reactor wall, supplied by electricity or alternative fuels (LEILAC2 Project, 2023). Resistance-heated rotary kilns are subject to scalability constraints due to the decreasing surface-to-volume ratio at larger sizes, which may limit heat transfer from externally mounted heating elements. Various technical solutions, including the integration of additional internal heating elements, have been proposed to mitigate these limitations (Li et al., 2014).

In the present study, we consider an electrically-heated rotary kiln where both calcination and clinkerization occur at 1000°C, in line with RC-BCC production requirements. The kiln is assumed to use indirect resistance heating, where the electric heating elements are placed around the kiln shell and heat is transferred through the steel wall to the raw material, as illustrated in Pisciotta et al. (2022). Hence, CO_2 emissions arise solely from limestone calcination, generating a high-CO_2 stream that is suitable for subsequent carbon utilization processes, e.g., mineral carbonation. A thermal efficiency of 60% is assumed to account for conductive losses through the kiln shell and insulation layers (Stemmermann et al., 2024).

2.2.2. Oxyfuel-fired rotary kiln

Oxyfuel combustion involves burning fuel with nearly pure oxygen instead of air (Pisciotta et al., 2022). When carbon-based fuels are used, the resulting flue gas consists mainly of CO_2 and H_2O, which can be separated more easily than in conventional air combustion systems (Ditaranto and Bakken, 2019).

Integrating oxyfuel combustion in the cement industry has been widely investigated for both retrofitting and new plant designs (Faria et al., 2022; International Energy Agency-Greenhouse Gas R&D Programme (IEA-GHG), 2013; Plaza et al., 2020; Rodríguez et al., 2012; ECRA, 2009). In this study, we consider an oxyfuel-fired rotary kiln operating at 1000°C, identical to the electrically-heated rotary kiln configuration, to enable the production of RC-BCC. Moreover, we assume that the oxyfuel-fired rotary kiln is compatible with various fuels, including natural gas, hydrogen, and biomass. As in Stemmermann et al. (2024), we assume a thermal efficiency of 50% for the oxyfuel-fired rotary kiln. Further details regarding oxygen supply, flue gas handling, and CO_2 purification are provided in Section 2.3.

2.3. Carbon capture: Oxyfuel combustion

Oxyfuel combustion is one of the most promising carbon capture technologies in the cement industry (Faria et al., 2022). Oxygen is typically supplied by an air separation unit (ASU). In addition, it can also be supplied as a by-product from water electrolysis.

The flue gas stream is highly concentrated in CO_2 due to the absence of nitrogen. After combustion, the hot flue gas is cooled by heat exchange in a condenser unit (C-OXY). The resulting stream is then split: a fixed fraction of 55%, selected as a representative value within the range reported for retrofit oxyfuel systems (International Energy Agency-Greenhouse Gas R&D Programme (IEA-GHG), 2013), is recycled to dilute the oxygen feed and maintain a stable flame temperature (Buhre et al., 2005; Voldsund et al., 2018), while the remaining 45% is directed to a carbon purification unit (CPU) for removal of residual oxygen and other minor impurities. The electricity requirements for the ASU and CPU are taken as 226 kWh per tonne of O_2 and 122.2 kWh per tonne of CO_2, respectively, based on data from Voldsund et al. (2018). These electricity demands are included in the plant-wide electricity balance. Similarly to our prior work (Ojeda-Paredes et al., 2025), only the capital expenditures for the ASU, condenser (C_OXY), and CPU units are considered in the economic assessment. Additionally, we assume a CO_2 capture rate of 90%. The remaining 10% of CO_2 emissions are released to the atmosphere, incurring CO_2 certificate costs (see Section 2.8) and contributing to the total direct emissions of the system (see Section 2.9).

2.4. Carbon capture and utilization: Mineral carbonation

Captured CO_2 can be used in carbon capture and utilization (CCU) technologies. In particular, mineral carbonation (MC) is considered a suitable technology for applications in the construction industry (Zajac et al., 2021; Sanna et al., 2014). In this technology, captured CO_2 reacts with alkaline or alkaline-earth oxides, such as magnesium oxide (MgO) and calcium oxide (CaO), to produce stable carbonates (Miller, 2011; Vanderzee and Zeman, 2018). Depending on the reaction mechanism, MC processes can be classified into two main categories: indirect and direct carbonation (Cuéllar-Franca and Azapagic, 2015).

Indirect MC involves multi-step processes, including metal extraction, metal hydration and subsequent carbonation (Cuéllar-Franca and Azapagic, 2015). Although capable of producing high-purity carbonates, indirect MC typically requires additional chemical inputs and complex process units, leading to high capital and operational costs (Zajac et al., 2022). In contrast, direct MC is performed as a single-step process, where CO_2 interacts directly with the mineral feedstock, allowing for simultaneous extraction and carbonate precipitation (Cuéllar-Franca and Azapagic, 2015). Direct MC can be implemented either in a gas–solid or aqueous-solid carbonation. In gas–solid systems, CO_2 is contacted with metal oxide feedstock in a reactor at elevated temperature to enhance reaction kinetics (Thonemann et al., 2022; Song et al., 2019). In aqueous systems, CO_2 is bubbled into a suspension of mineral-rich solid feedstock. The dissolution of CO_2 lowers the pH, which promotes the release of metal ions from the solid phase. These ions subsequently react with carbonate species in solution, leading to precipitation of stable carbonates (Chakraborty and Jo, 2018; Thonemann et al., 2022). Although aqueous systems typically achieve high reaction efficiency, they require additional energy for downstream separation and drying of the produced carbonates. The technology readiness level (TRL) of mineral carbonation ranges from 3 to 7, i.e., from laboratory research to pilot plant (Pedraza et al., 2021), depending on the mineral carbonation mechanism utilized. For example, the direct aqueous mineral carbonation process developed by Mineral Carbonation International (MCi) has reached TRL 7 (Back et al., 2022). Industrial efforts to develop mineral carbonation technologies for the production of supplementary cementitious materials are also emerging (e.g., Co–Reactive (2024)).

In the present study, we consider mineral carbonation for three key purposes: (i) to utilize the concentrated CO_2 captured from RC-BCC production, (ii) to valorize the coarse fraction of waste concrete, and (iii) to produce carbonated aggregates that can be stored or used in concrete production. Hence, we include both direct aqueous and gas–solid mineral carbonation configurations as process options in the superstructure. The recycled aggregates (rA) are assumed to contain 6.5% CaO. For gas–solid carbonation, a fluidized bed reactor (GAS-CARB) is used and supplied with thermal energy from an electric boiler (EL-BOIL). For the aqueous carbonation route, a stirred tank reactor (AQ-CARB) followed by a separation and drying stage (AQ-SEP) is considered. Electricity consumption for the aqueous route is assumed as 5 kWh per tonne of CO_2 in the reactor and 350 kWh per tonne of carbonated product for post-treatment (Sanna et al., 2012; Iizuka et al., 2004). At the system level, we assume that sufficient amounts of waste concrete, in particular recycled aggregates, are locally available and technically suitable (e.g., with respect to water content and particle size) for the considered mineral carbonation routes, such that mineral carbonation is constrained by the CO_2 production rate from clinker production. Under this assumption, all captured CO_2 can be utilized at the plant level, provided adequate waste availability. This represents a favorable but location-dependent configuration, in which the availability of suitable waste concrete exceeds the amount required to mineralize the CO_2 captured from RC-BCC production. In practical applications, this assumption would require a site-specific assessment of waste concrete availability and logistics.

2.5. Concrete production

Concrete production involves the basic processes of batching and mixing. During batching, raw materials are proportioned to achieve the desired end-product characteristics (Griffiths et al., 2023). Next, the materials are blended to produce ready mix concrete, i.e., concrete that is mixed at a central plant prior to delivery. Mixing can occur at the concrete plant, in the transport truck, or can happen partially in the truck and partially at the plant (Kermeli et al., 2011). Different types of concrete can be formulated by adjusting the proportions of cement, aggregates, and water, depending on specific performance requirements such as compressive strength, durability, and thermal resistance (Griffiths et al., 2023).

In this study, we focus on the production of concrete type C25/30, i.e., 28-day compressive strength between 25 and 30 MPa, since it is one of the most commonly produced concrete grades in Germany, based on data from 2023 (Statista, 2024). We consider the mass composition for this type of concrete as 12.4% cement, 82.42% aggregates (fine and coarse), and 5.18% water, according to Bundesministerium für Wohnen, Stadtentwicklung und Bauwesen (2024). Based on previous

studies (Stemmermann et al., 2022, 2024), we consider that RC-BCC can partially substitute Portland cement, with a maximum replacement ratio of 50% by weight. Due to the maximum production capacity of RC-BCC of 50 kt per year (for an operational period of 300 days), we estimate a concrete production throughput of approximately 115 tonnes per hour, equivalent to around 50 m^3/h. The concrete production unit (BATCH-MIX) is modeled as a central batching plant, where raw materials are prepared and mixed on site prior to delivery. Electricity consumption, primarily associated with mixing, is assumed to be 1.6 kWh per tonne of concrete, based on values reported in Kermeli et al. (2011).

2.6. Energy system

Fossil fuels have been the primary energy source in cement production to provide the high temperatures required in rotary kilns. Currently, alternative fuels such as natural gas, hydrogen and biomass have gained interest in this sector due to their potential to reduce combustion-related CO_2 emissions. These options have been studied and tested at industrial scale (Juangsa et al., 2022; El-Emam and Gabriel, 2021; Nhuchhen et al., 2021; Ozturk and Dincer, 2022; Walker et al., 2009; Smith, 2003).

In this study, we consider natural gas, biomass, and hydrogen as potential fuels to supply heat to the oxyfuel-fired rotary kiln. Hydrogen may be either purchased or produced on site via water electrolysis. For electrolytic hydrogen production, we include two commercially relevant electrolyzer technologies: alkaline electrolyzer (AEL) and proton exchange membrane electrolyzer (PEMEL), similar to our prior work (Ojeda-Paredes et al., 2025). The average efficiency of both systems, based on the lower heating value (LHV), is assumed to be 67% for AEL and 64% for PEMEL (Buttler and Spliethoff, 2018). The capital expenditure (CAPEX) for each electrolyzer is estimated at 1180 EUR/kW_{el} for AEL and 1640 EUR/kW_{el} for PEMEL, with fixed operating costs set at 4% of the investment costs (van Leeuwen and Zauner, 2018).

To model the combustion reactions, we assume natural gas as pure methane (CH_4) (Grammelis et al., 2016) and biomass as wood chips with a chemical composition of $CH_{1.44}O_{0.66}$ (Nussbaumer, 2003). The corresponding lower heating values and stoichiometric combustion equations are detailed in the supporting materials.

2.7. Storage units

To provide operational flexibility, we consider storage units for both solid and gaseous streams. Solid storage units are included for the fine and coarse fractions of waste concrete, the raw meal after milling, the clinker after cooling, the ground recycled belite cement clinker (gRC-BCC), and the carbonated aggregates from mineral carbonation. In addition, hydrogen produced via electrolysis, oxygen from the air separation unit or as by-product of electrolysis, and CO_2 from oxyfuel combustion or limestone calcination are assumed to be stored in pressurized tanks.

Specifically, for H_2 storage, a pressure of 200 bar is assumed, requiring the installation of a two-stage compression unit (H2-COMP) to raise the pressure from 30 to 200 bar, following Chardonnet et al. (2017). Gaseous O_2 can be stored in buffer tanks at 30 bar (Assunção et al., 2025). Therefore, we consider a pressurized storage tank and a three-stage compression system (see Section 3 of supporting materials) to increase the pressure from 1.8 bar (gaseous O_2 produced from ASU (Global CCS Institute, 2018)) to 30 bar. CO_2 is typically stored as a liquid in medium pressure tanks. Based on commercial specifications (Chart Industries, 2021), we consider a storage pressure of 25 bar. The inlet pressure of the CO_2 compressor varies depending on its source, i.e., CO_2 from limestone calcination from the electrically-heated rotary kiln is at atmospheric pressure (1.01 bar), whereas CO_2 from the oxyfuel-fired rotary kiln is at 16.5 bar due to the upstream carbon purification unit (Jackson and Brodal, 2019). The electricity demand for each compressor, and the investment costs for compressors and storage units are reported in the supporting materials.

2.8. Commodities prices and CO_2 certificate price

The commodities used in the system for which we calculate the operational costs include electricity, limestone, biomass, hydrogen, natural gas, Portland cement, and fine and coarse aggregates. For electricity, we consider day-ahead prices from the German electricity market for the year 2024 (Bundesnetzagentur|SMARD.de, 2024), implemented as time-varying parameters in the model. The prices of limestone and aggregates (fine and coarse) are calculated by dividing the total sales value by the production volume in 2024 (Information und Technik Nordrhein-Westfalen (IT.NRW), 2024). For Portland cement, we consider the average price reported in Germany for 2024 (OneStone Consulting, 2024). Regarding fuels, the natural gas price is based on average prices for large-scale industrial consumers in 2024 (Bundesnetzagentur and Bundeskartellamt, 2024). Green hydrogen is modeled as an externally supplied commodity with an assumed purchase cost. Biomass price, based on wood chips with 35% moisture content, is obtained from the German biomass market (C.A.R.M.E.N. e.V., 2024).

When the oxyfuel-fired rotary kiln is operated, 10% of the generated CO_2 is not captured, based on the assumed capture efficiency of 90%. For this fraction, we consider the payment of CO_2 certificates, i.e., the average European Union Allowances (EUA) price in 2024 (EEX, 2024).

The economic parameters, including reference prices and assumptions, are summarized in Section 1 and Tab. 1 of the supporting materials.

2.9. Direct and indirect emissions

To evaluate the global warming impact of the system, we account for both direct and indirect CO_2 emissions.

Direct CO_2 emissions arise from the calcination of limestone in the kiln and from the combustion of fossil fuels, i.e., we only account for emissions from natural gas, as biomass may be considered a carbon-neutral fuel (Abbasi and Abbasi, 2010).

Indirect emissions are associated with the upstream production and transport of commodities. For electricity, we consider the emission factor of the German electricity mix in 2024, which reflects a fossil fuel share of 41% (Icha and Lauf, 2025). For externally supplied green hydrogen, we assume that it is produced via electrolysis using renewable electricity, and we use the upstream emission factor for wind-powered hydrogen production reported in Bhandari et al. (2014) and Spath and Mann (2004). For biomass and natural gas, we account for upstream emissions related to production and transportation. For aggregates, we apply emission factors for manufactured sand (fine aggregates) and crushed stone (coarse aggregates), both taken from Zhu et al. (2023). For limestone, we consider the value from Bolte et al. (2019) that considers the transportation and grinding to produce limestone for use in cement production. For Portland cement, we consider the global warming impact of Portland cement produced in Germany with a clinker content of 90% (Verein Deutscher Zementwerke e.V. (VDZ), 2022). All environmental parameter values are provided in Section 1 and Tab.2 of the supporting materials.

3. Model and problem formulation

In the following, we formulate a model for the optimal design and operation of the low-carbon concrete production process and its energy supply system. Similar to our previous work (Ojeda-Paredes et al., 2025), our model is based on mass and energy balances, conversion models (e.g., stoichiometry), constitutive equations, nonlinear cost correlations and additional linear constraints representing design and operational limits. However, unlike in the previous work, we consider a discrete-time representation (Floudas and Lin, 2004) and assume a quasi-stationary system behavior, meaning that the system immediately reaches new steady-state conditions after an operational

change (Voll et al., 2013). The model is implemented in our open-source framework for energy systems optimization COMANDO (Langiu et al., 2021). We use COMANDO because it allows component-oriented modeling, superstructure-based optimization and the formulation of two-stage stochastic optimization problems, which are well suited to the integrated design and operation problem addressed in this work. Using the built-in automatic linearization, which relies on the convex-combination method (Vielma et al., 2010), a mixed-integer linear program (MILP) is obtained. The resulting MILP is a bi-objective problem that considers both economic and environmental objectives, i.e., total annualized costs (TAC) and global warming impact (GWI), respectively. The size of the linearized superstructure MILP depends on the number of representative days considered in the temporal aggregation. For the representative-day configurations considered in this work, i.e., 4 to 20 clusters, the MILP size ranges from 49,407 to 290,280 constraints, 33,324 to 186,160 continuous variables, and 34,306 to 159,124 discrete variables. The resulting MILPs are solved using Gurobi 9.5.1 (Gurobi Optimization, LLC, 2020) with a relative optimality tolerance of 0.1% on a desktop PC with an Intel i7-8700 processor and 32 GB RAM, running Windows 10 Enterprise LTSC.

3.1. Clustering of electricity price data and time discretization

We consider German day-ahead electricity prices for 2024 at hourly resolution (8784 h, 366 days). To reduce the size of the optimization problem while preserving variability in daily price profiles, we adopt a typical-day representation widely used in energy systems optimization (Thiran et al., 2023).

Daily profiles (24 consecutive hourly values) are clustered with k-means (MacQueen, 1967) using the scikit-learn package in Python (Pedregosa et al., 2011). To assess the effect of the temporal aggregation, we solve the quasi-stationary model for different numbers of representative days, denoted by K, with $K \in \{4, 6, 8, 10, 12, 14, 16, 18, 20\}$. For a given value of K, the set of clusters is defined as $\mathcal{K} = \{1, \dots, K\}$. Each cluster $k \in \mathcal{K}$ is characterized by a centroid (average 24-hour price pattern) and a weight ω_k which is proportional to the number of days in the full year represented by that cluster.

For illustration, Fig. 2 shows the representative daily electricity price profiles obtained for $K = 6$, together with their corresponding weights expressed as probabilities of occurrence. This example illustrates how the clustering approach represents common daily price profiles with moderate intra-day variations, while also capturing rare profiles with pronounced price peaks. In this case, the dominant cluster (Cluster 1, $p_1 = 34.7\%$) shows moderate prices between 80 and 150 EUR/MWh, whereas Cluster 6 captures extreme price volatility, with prices ranging from 100 to 950 EUR/MWh within a single day.

Cement plants typically operate for about 300 to 310 days per year, due to annual shutdowns for major maintenance and repairs (Noche and Elhasia, 2013). Accordingly, for each considered value of K, we rescale the cluster weights from the full leap year (366 days in 2024) to 300 operating days by enforcing

$$\sum_{k \in \mathcal{K}} \omega_k = 300, \tag{1}$$

i.e., the individual weights ω_k are rescaled as

$$\omega_k = \omega_k^{(366)} \cdot \frac{300}{366} \qquad \forall k \in \mathcal{K}. \tag{2}$$

Finally, for each value of K, we define the model time set as

$$\mathcal{T} = \mathcal{K} \times \mathcal{H}, \tag{3}$$

where $\mathcal{K} = \{1, \dots, K\}$ is the set of representative days and $\mathcal{H} = \{1, \dots, 24\}$ is the set of hourly periods within a day. In the following formulation, $\mathcal{K}$ and $\mathcal{T}$ refer to the cluster set and time set associated with the respective value of K.

3.2. Balance and constitutive equations

Similar to our previous superstructure approach (Ojeda-Paredes et al., 2025), we represent the process and energy system units as unit operations, which are referred to as components in the mathematical formulation. We define the set of components $\mathcal{C}$ containing the set of mixers ($\mathcal{X}$), splitters ($\mathcal{L}$), conversion units ($\mathcal{U}$), electricity-based units ($\mathcal{E}$), thermal units ($\mathcal{Q}$), and storage units ($\mathcal{W}$). Since storage units are modeled separately through the state-of-charge equations introduced in Section 3.4, the stationary mass balance is written only for the non-storage components. Accordingly, we further define the set of non-storage components $\mathcal{C}^{ns}$, which contains mixers, splitters, conversion units, electricity-based units, and thermal units. All time-dependent variables are indexed by the cluster–hour pair $(k, h) \in \mathcal{T}$ introduced in Section 3.1. The stationary energy balance for a non-storage component c at time step (k, h) is expressed as

$$\sum_{i \in \mathcal{F}_c^{E,in}} \dot{E}_{c,i,k,h}^{in} = \sum_{j \in \mathcal{F}_c^{E,out}} \dot{E}_{c,j,k,h}^{out} \qquad \forall c \in \mathcal{C}^{ns},\ (k,h) \in \mathcal{T} \tag{4}$$

where $\dot{E}_{c,i,k,h}^{in}$ and $\dot{E}_{c,j,k,h}^{out}$ denote the incoming and outgoing energy flows, respectively. For each component c, the incoming and outgoing flows are determined by the connectivity of the superstructure shown in Fig. 1. Accordingly, we define the sets $\mathcal{F}_c^{E,in}$ and $\mathcal{F}_c^{E,out}$ for the incoming and outgoing energy flows of component c, respectively. An output energy flow $\dot{E}_{c,j,k,h}^{out}$ can be determined using the efficiency of conversion $\eta_{c,i\to j}$ and the incoming energy flow $\dot{E}_{c,i,k,h}^{in}$ as follows:

$$\dot{E}_{c,j,k,h}^{out} = \eta_{c,i\to j} \cdot \dot{E}_{c,i,k,h}^{in} \tag{5}$$

The electrical power demand $\dot{S}_{el,k,h}$ is given by

$$\dot{S}_{el,k,h} = \sum_{c \in \mathcal{E}} \dot{E}_{c,k,h}^{in,el}, \tag{6}$$

where $\dot{E}_{c,k,h}^{in,el}$ represents the electrical (el) power demand of a component c from the set $\mathcal{E}$ of electricity-based components.

The stationary mass balance for a non-storage component c at time step (k, h) is formulated as

$$\sum_{m \in \mathcal{M}} \dot{S}_{m,c,k,h} + \sum_{i \in \mathcal{F}_c^{M,in}} \dot{M}_{c,i,k,h}^{in} = \sum_{j \in \mathcal{F}_c^{M,out}} \dot{M}_{c,j,k,h}^{out} + \sum_{n \in \mathcal{N}} \dot{S}_{n,c,k,h}$$
$$\forall c \in \mathcal{C}^{ns},\ (k,h) \in \mathcal{T}. \tag{7}$$

Here, the input mass flows originating from other components $\dot{M}_{c,i,k,h}^{in}$ and from sources $\dot{S}_{m,c,k,h}$ are equal to the output mass flows leaving to other components $\dot{M}_{c,j,k,h}^{out}$ and to sinks $\dot{S}_{n,c,k,h}$. For each component c, the incoming and outgoing mass flows are determined by the connectivity of the superstructure shown in Fig. 1. Accordingly, we define the sets $\mathcal{F}_c^{M,in}$ and $\mathcal{F}_c^{M,out}$ for the incoming and outgoing mass flows of component c, respectively. The set $\mathcal{M}$ contains the material sources (i.e., concrete waste, limestone, hydrogen, natural gas, biomass, Portland cement, fine aggregates and coarse aggregates), and the set $\mathcal{N}$ contains all the sinks (i.e., concrete, flue gases, water, biogenic CO_2 emissions, and non-biogenic CO_2 emissions).

In oxyfuel combustion, part of the kiln exhaust is returned to the burner in order to moderate flame temperature. In the superstructure this loop is represented by a splitter–mixer pair. For a mixer $x \in \mathcal{X}$, the outflow $\dot{M}_{x,k,h}^{out}$ can be calculated by summing up the inflow streams $\dot{M}_{x,i,k,h}^{in}$, i.e.,

$$\dot{M}_{x,k,h}^{out} = \sum_{i \in \mathcal{F}_x^{M,in}} \dot{M}_{x,i,k,h}^{in}. \tag{8}$$

For a splitter $l \in \mathcal{L}$,

$$\sum_{j \in \mathcal{F}_l^{M,out}} \dot{M}_{l,j,k,h}^{out} = \dot{M}_{l,k,h}^{in}, \tag{9}$$

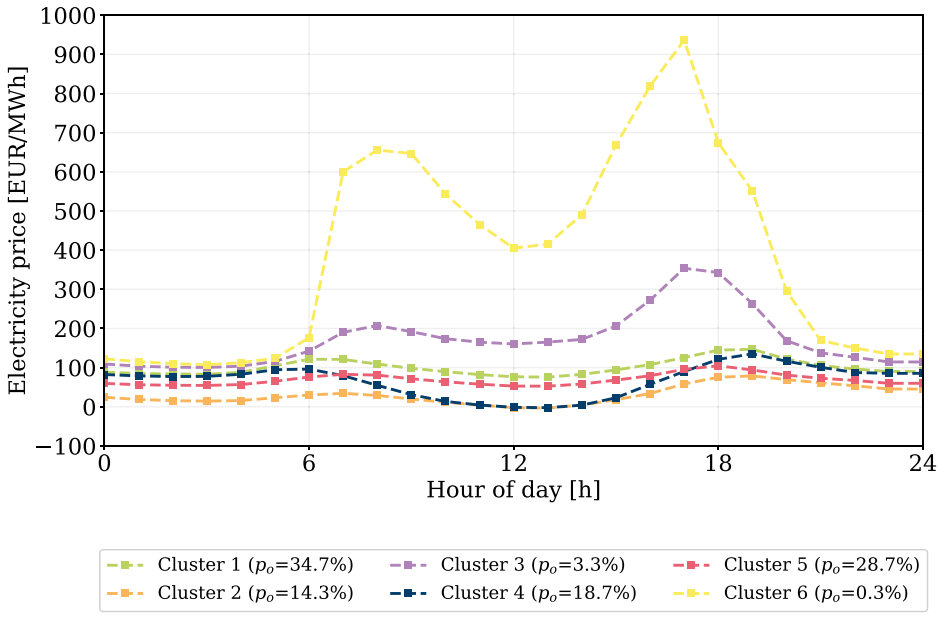

Fig. 2. Illustrative electricity price profiles of representative days for $K = 6$.

and the outflow $\dot{M}^{out}_{l,j,k,h}$ is calculated based on the known split fractions $\zeta_{l,j}$ by

$$\dot{M}^{out}_{l,j,k,h} = \zeta_{l,j} \cdot \dot{M}^{in}_{l,k,h} \qquad \forall j \in \mathcal{F}^{M,out}_{l}. \tag{10}$$

A conversion unit represents a unit operation in which a chemical reaction takes place. The set of conversion units $\mathcal{U}$ consists of the rotary kiln, the carbonator, and the AEL and PEMEL electrolyzers. A conversion unit u is modeled as

$$\dot{M}^{out}_{u,j,k,h,g} = \dot{M}^{in}_{u,i,k,h,e} \cdot \left(\frac{w_g}{w_e}\right) \cdot \left(\frac{\nu_{u,g}}{\nu_{u,e}}\right). \tag{11}$$

In a conversion unit u, a product g from the set of products $\mathcal{G}_u$ is generated from the conversion of a reactant e from the set of reactants $\mathcal{E}_u$. The terms $\nu_{u,g}$ and $\nu_{u,e}$ represent the stoichiometric coefficients of the product and the reactant, respectively. The molecular weights of the product and the reactant are denoted as w_g and w_e, respectively.

Additionally, the energy input or output ($\dot{E}^{in/out}_{u,heat,k,h}$) due to endothermic or exothermic reactions, respectively, is calculated as

$$\dot{E}^{in/out}_{u,heat,k,h} = \left(\frac{\dot{M}^{in}_{u,i,k,h,e}}{w_e}\right) \cdot \Delta H_u, \tag{12}$$

where ΔH_u is the heat of reaction taking place in the conversion unit u.

The set of thermal units $\mathcal{Q}$ includes the components in which heat is transferred without involving chemical reactions, such as the condenser in oxyfuel combustion, the gas–gas heat exchanger for heat recovery, and the preheater and cooler in belite cement production. In a condenser q, a gaseous mixture is cooled to condense water vapor. The remaining gases (oxygen and carbon dioxide) are sent to the carbon purification unit. The stationary energy balance of the condenser is based on the sensible heat of the fluid streams and the heat removed, and is given by

$$\dot{E}^{in}_{q,k,h(\text{gaseous mixture})} = \dot{E}^{out}_{q,k,h(\text{residual gases})} + \dot{E}^{out}_{q,k,h(\text{liquid water})} + \dot{E}^{out}_{q,heat,k,h}, \tag{13}$$

where $\dot{E}^{in}_{q,k,h(\text{gaseous mixture})}$, $\dot{E}^{out}_{q,k,h(\text{residual gases})}$, and $\dot{E}^{out}_{q,k,h(\text{liquid water})}$ represent the enthalpies of the respective streams. These are computed from their mass flow rates, specific heat capacities, temperatures, and aggregate states. The term $\dot{E}^{out}_{q,heat,k,h}$ represents the heat removed during the condensation process.

For a heat exchanger q, heat is recovered from the hot gas stream (CO_2-rich gas stream in the oxyfuel-fired rotary kiln, or pure CO_2 in the electrically-heated rotary kiln) and transferred to an air stream used for preheating. The energy balance is formulated based on the sensible heat as

$$\dot{M}^{in/out}_{q,k,h,hot} \cdot c_{q,hot} \cdot \Delta T_{q,hot} = \dot{M}^{in/out}_{q,k,h,cold} \cdot c_{q,cold} \cdot \Delta T_{q,cold}, \tag{14}$$

where $\dot{M}^{in/out}_{q,k,h,hot} = \dot{M}^{in}_{q,k,h,hot} = \dot{M}^{out}_{q,k,h,hot}$ and $\dot{M}^{in/out}_{q,k,h,cold} = \dot{M}^{in}_{q,k,h,cold} = \dot{M}^{out}_{q,k,h,cold}$ denote the mass flow rates of the hot and cold streams, respectively, which are conserved across the exchanger. The specific heat capacities $c_{q,hot}$ and $c_{q,cold}$ are evaluated at the arithmetic mean of the corresponding inlet and outlet temperatures of each stream. The temperature differences $\Delta T_{q,hot}$ and $\Delta T_{q,cold}$ represent the inlet–outlet temperature changes on the hot and cold sides, respectively.

In the case of the preheater and the cooler, heat is transferred between a gas and a solid stream. Assuming no heat losses to the environment, the energy balance is written as

$$\dot{E}^{in}_{q,k,h(\text{solids})} + \dot{E}^{in}_{q,k,h(\text{gas})} = \dot{E}^{out}_{q,k,h(\text{solids})} + \dot{E}^{out}_{q,k,h(\text{gas})}. \tag{15}$$

Here, each energy term $\dot{E}$ corresponds to the enthalpy flow of the respective stream, calculated using its mass flow, heat capacity, and temperature. In the preheater, the solid and gas streams correspond to raw meal and air, respectively. In the cooler, they correspond to belite clinker and air.

3.3. Material composition constraints

To capture the effect of variable material composition for recycled belite cement clinker (RC-BCC) and concrete production, we impose composition bounds as

$$0.40\, m^{\text{rm}} \le m^{\text{rCF}} \le 0.50\, m^{\text{rm}}, \tag{16}$$

$$0.50\, m^{\text{rm}} \le m^{\text{lime}} \le 0.60\, m^{\text{rm}}, \tag{17}$$

$$0.50\, m^{\text{cem}} \le m^{\text{PC}} \le 1.00\, m^{\text{cem}}, \tag{18}$$

$$0.00\, m^{\text{cem}} \le m^{\text{RC-BCC}} \le 0.50\, m^{\text{cem}}. \tag{19}$$

Here, m^{rm} is the raw meal for RC-BCC production, consisting of a mass of limestone m^{lime} and recycled concrete fines (rCF) m^{rCF}, while m^{cem} is

the cement blend used for concrete production, composed of Portland cement (PC) m^{PC} and RC-BCC $m^{\mathrm{RC-BCC}}$. The totals are calculated by

$$m^{\mathrm{rm}} = m^{\mathrm{rCF}} + m^{\mathrm{lime}}, \tag{20}$$

$$m^{\mathrm{cem}} = m^{\mathrm{PC}} + m^{\mathrm{RC-BCC}}, \tag{21}$$

which are added as equality constraints. The composition is optimized in the steady-state design (cf. Section 3.2). In the subsequent quasi-stationary integrated design and scheduling model, the fractions from the steady-state design are treated as fixed parameters, such that the hourly flows are calculated by

$$\dot{M}^{in}_{\mathrm{batch-mix,PC},k,h} = \phi^{\mathrm{PC}} \cdot \dot{M}^{in}_{\mathrm{batch-mix,cem},k,h}, \tag{22}$$

$$\dot{M}^{in}_{\mathrm{batch-mix,RC-BCC},k,h} = \phi^{\mathrm{RC-BCC}} \cdot \dot{M}^{in}_{\mathrm{batch-mix,cem},k,h}, \tag{23}$$

$$\dot{M}^{in}_{\mathrm{rm-mill,rCF},k,h} = \phi^{\mathrm{rCF}} \cdot \dot{M}^{in}_{\mathrm{rm-mill,rm},k,h}, \tag{24}$$

$$\dot{M}^{in}_{\mathrm{rm-mill,lime},k,h} = \phi^{\mathrm{lime}} \cdot \dot{M}^{in}_{\mathrm{rm-mill,rm},k,h}, \tag{25}$$

where ϕ^{PC}, $\phi^{\mathrm{RC-BCC}}$, ϕ^{rCF} and ϕ^{lime} are the design fractions, which are applied consistently across all cluster–hour pairs $(k,h) \in \mathcal{T}$, i.e., we do not assume that the composition would be time-varying.

3.4. Design and operational constraints

We include a binary decision variable x_c that indicates whether the component c is installed. The nominal size D_c^{nom} of each component $c \in \mathcal{C}$ is constrained by

$$x_c D_c^{min} \le D_c^{nom} \le x_c D_c^{max}, \tag{26}$$

where D_c^{min} and D_c^{max} are the minimum and maximum size, respectively. Note that the nominal size can be expressed in terms of mass or energy, depending on the component type and the investment cost correlation. For storage units $w \in \mathcal{W}$, the nominal size represents the installed storage capacity and corresponds to the maximum storage level.

To enable flexible operation of non-storage components, we introduce the variable $D^{ope}_{c,k,h}$ to represent their operating level. It is bounded by

$$y_{c,k,h} D_c^{nom} p_c^{min} \le D^{ope}_{c,k,h} \le y_{c,k,h} D_c^{nom} \qquad \forall c \in C^{ns},\ (k,h) \in \mathcal{T} \tag{27}$$

where $y_{c,k,h}$ is the binary decision to operate the non-storage component c and p_c^{min} is the minimal part-load factor. Depending on the component model, $D^{ope}_{c,k,h}$ may correspond to a production rate or to an operating load. For example, for the rotary kiln, $D^{ope}_{c,k,h}$ represents the production rate, whereas for the CO_2 compressor it represents the operating load. Note that Eq. (27) contains a bi-linear term that is reformulated based on (Glover, 1975) as

$$z_{c,k,h} \ge y_{c,k,h} D_c^{min} \qquad \forall c \in C^{ns},\ (k,h) \in \mathcal{T}, \tag{28}$$

$$z_{c,k,h} \le y_{c,k,h} D_c^{max} \qquad \forall c \in C^{ns},\ (k,h) \in \mathcal{T}, \tag{29}$$

$$z_{c,k,h} \ge D_c^{nom} - D_c^{max}(1 - y_{c,k,h}) \qquad \forall c \in C^{ns},\ (k,h) \in \mathcal{T}, \tag{30}$$

$$z_{c,k,h} \le D_c^{nom} - D_c^{min}(1 - y_{c,k,h}) \qquad \forall c \in C^{ns},\ (k,h) \in \mathcal{T}, \tag{31}$$

where $z_{c,k,h}$ acts as an auxiliary variable for the product of the binary $y_{c,k,h}$ and the continuous variable D_c^{nom}.

Finally, Eq. (27) is reformulated and expressed as

$$z_{c,k,h} p_c^{min} \le D^{ope}_{c,k,h} \le z_{c,k,h} \qquad \forall c \in C^{ns},\ (k,h) \in \mathcal{T}. \tag{32}$$

The operation rate $D^{ope}_{c,k,h}$ of a non-storage component $c \in C^{ns}$ is linked to the output mass or energy flow by

$$D^{ope}_{c,k,h} = \dot{M}^{out}_{c,j,k,h} \text{ or} \tag{33}$$

$$D^{ope}_{c,k,h} = \dot{E}^{out}_{c,j,k,h}\text{ , respectively.} \tag{34}$$

We allow the storage of various products and intermediates. Specifically, the set $\mathcal{W}$ includes storages for concrete waste (fines and coarse), raw meal, hydrogen, oxygen, carbon dioxide, aggregates, belite binder, and belite cement. All storage variables are indexed by the cluster–hour pair $(k,h) \in \mathcal{T}$. The state of charge (SOC) of each storage unit w is calculated, similarly to (Röben et al., 2021), as

$$SOC_{w,k,h} = SOC_{w,k,h-1} + (\dot{M}^{in}_{w,k,h} - \dot{M}^{out}_{w,k,h})\Delta t \qquad \forall w \in \mathcal{W},\ k \in \mathcal{K},\ h = 1, \dots, 24, \tag{35}$$

where $SOC_{w,k,h}$ represents the state of charge that is based on the state of charge $SOC_{w,k,h-1}$ from the previous time step, $\dot{M}^{in}_{w,k,h}$ and $\dot{M}^{out}_{w,k,h}$ denote the input and output material flows to and from the storage, respectively, and $\Delta t = 1$ h.

Additionally, we consider the following cyclical storage constraints:

$$SOC_{w,k,24} = SOC_{w,k,0} \qquad \forall w \in \mathcal{W},\ k \in \mathcal{K}, \tag{36}$$

$$SOC_{w,k+1,0} = SOC_{w,k,0} \qquad \forall w \in \mathcal{W},\ k = 1, \dots, K-1. \tag{37}$$

Here, Eqs. (36) and (37) are introduced so that the final state of charge is identical to the initial state of charge within each typical day and that all typical days share the same initial SOC. Thus, the storage model captures short-term intra-day buffering within each representative day.

3.5. Objectives

The economic and environmental objectives of the optimization problem are the total annualized costs (TAC) and the global warming impact (GWI), respectively. The TAC is computed as

$$TAC = \sum_{c \in \mathcal{C}} (CX_c \cdot CRF + OX_c^{fix}) + \sum_{k \in \mathcal{K}} \omega_k \sum_{h \in \mathcal{H}} \Big(\sum_{s \in S} OX^{var}_{s,k,h} + OX^{var}_{CO_2,k,h} \Big) \Delta t, \tag{38}$$

where ω_k are the cluster weights, CX_c represents the capital expenditure (CAPEX) for component c annualized by the capital recovery factor CRF. The term OX_c^{fix} accounts for fixed operating expenditures, i.e., maintenance costs. Variable operating expenditures include $OX^{var}_{s,k,h}$, associated with the consumption of commodity $s \in S$, and $OX^{var}_{CO_2,k,h}$ from the payment of CO_2 certificates. The set of commodities S includes material sources $m \in \mathcal{M}$ and electricity $\dot{S}_{el,k,h}$ taken from the grid.

The capital expenditure CX_c for each component c is estimated by a power-law correlation based on nominal capacity (Smith, 2016) as

$$CX_c = x_c \cdot CX_c^{ref} \cdot \left(\frac{D_c^{nom}}{D_c^{ref}} \right)^{\alpha} \cdot \left(\frac{CEPCI^{2024}}{CEPCI^{ref}} \right) \forall c \in C, \tag{39}$$

where α is the scale factor, and CX_c^{ref} and D_c^{ref} denote the reference cost and nominal capacity, respectively. CAPEX CX_c values are updated to the base year 2024 using the Chemical Engineering Plant Cost Index (CEPCI), with $CEPCI^{2024}$ and $CEPCI^{ref}$ denoting to CEPCI values for the scenario year and reference year, respectively. Parameter values and index data can be found in the supporting materials. The capital recovery factor CRF converts the initial investment into an annualized cost, based on a project lifetime γ and a discount rate σ (see supporting materials), as follows

$$CRF = \frac{(1+\sigma)^{\gamma} \cdot \sigma}{(1+\sigma)^{\gamma} - 1}. \tag{40}$$

The fixed annual operating expenditure OX_c^{fix} is estimated as a fraction T_c^{fix} of the investment cost CX_c by

$$OX_c^{fix} = T_c^{fix} \cdot CX_c \quad \forall c \in C. \tag{41}$$

The variable operating expenditures arise from (i) the consumption of commodities $OX^{var}_{s,k,h}$ and (ii) the payment of CO_2 certificates $OX^{var}_{CO_2,k,h}$. These costs are calculated as

$$OX^{var}_{s,k,h} = p_{s,k,h} \cdot \dot{S}_{s,k,h} \qquad \forall s \in S,\ \forall (k,h) \in \mathcal{T}, \tag{42}$$

$$OX^{var}_{CO_2,k,h} = p_{CO_2,k,h} \cdot \dot{S}_{CO_2,k,h} \qquad \forall (k,h) \in \mathcal{T}, \tag{43}$$

with $\dot{S}_{s,k,h}$ the consumption rate of commodity s and $\dot{S}_{CO_2,k,h} \in \mathcal{N}$ the amount of fossil CO_2 emitted to the atmosphere, both at (k,h) and for $\Delta t = 1$ h. In our setup, only electricity prices can be time-varying, therefore,

$$p_{s,k,h} = \begin{cases} p_{el,k,h} & \text{for } s = el \text{ (electricity, hourly from cluster centroids),} \\ p_s & \text{for } s \neq el \text{ (constant in a scenario).} \end{cases}$$

The annual GWI is defined as

$$GWI = \sum_{k \in \mathcal{K}} \omega_k \sum_{h \in \mathcal{H}} \left(GWI^{dir}_{k,h} + \sum_{s \in S} GWI^{ind}_{s,k,h} - CS_{bio,k,h} \right) \cdot \Delta t. \tag{44}$$

Here, $GWI^{dir}_{k,h}$ represents the direct non-biogenic CO_2 emissions to the atmosphere at (k,h), $GWI^{ind}_{s,k,h}$ denotes the indirect impact associated with the use of commodity s, and $CS_{bio,k,h}$ represents the carbon credits attributed to the permanent storage of biogenic CO_2. Again, $\Delta t = 1$ h.

Note that the climate mitigation potential of carbon capture and utilization (CCU) systems depends significantly on the lifetime of the resulting products (Schlögl et al., 2018). Mineral carbonation enables long-term CO_2 storage by transforming CO_2 into stable solids (Metz et al., 2005). Baena-Moreno et al. (2019) emphasize that these carbonated solids, e.g., $CaCO_3$, can securely store CO_2 over extended periods without leakage risks. Thus, we assume that the captured CO_2, regardless of its fossil or biogenic origin, is converted into stable carbonates, thereby ensuring that the CO_2 remains isolated from the atmosphere in the long term.

As described in Section 2, two types of rotary kiln technologies are considered: (i) an oxyfuel-fired kiln and (ii) an electrically-heated kiln. In the latter case, CO_2 emissions originate solely from limestone calcination (process emissions), and we assume that 100% of this CO_2 can be captured and mineralized into carbonates. In contrast, the oxyfuel-fired kiln generates fossil CO_2 from both natural gas combustion and limestone calcination. A fraction of this CO_2 is released to the atmosphere due to the CO_2 capture rate of 90% of the carbon purification unit (ECRA, 2009). Therefore, the direct GWI term is calculated as

$$GWI^{dir}_{k,h} = EF_{NG} \cdot \dot{M}^{in}_{oxy-kiln,NG,k,h} + EF_{lime} \cdot \dot{M}^{in}_{oxy-kiln,lime,k,h} - CO^{fos,util}_{2,k,h} \quad \forall (k,h) \in \mathcal{T}, \tag{45}$$

where EF_{NG} and EF_{lime} are the emission factors for natural gas combustion and limestone calcination, respectively. $\dot{M}^{in}_{oxy-kiln,NG,k,h}$ and $\dot{M}^{in}_{oxy-kiln,lime,k,h}$ are the natural gas and limestone mass inflows to the oxyfuel-fired rotary kiln, respectively. $CO^{fos,util}_{2,k,h}$ is the amount of fossil CO_2 permanently stored via mineral carbonation.

The indirect GWI is calculated as

$$GWI^{ind}_{s,k,h} = EF^{ind}_s \cdot \dot{S}_{s,k,h} \ \forall s \in S, (k,h) \in \mathcal{T}, \tag{46}$$

where EF^{ind}_s is the upstream emission factor, and $\dot{S}_{s,k,h}$ is the commodity consumption rate. Direct and indirect emission factors can be found in the supporting materials.

Finally, carbon credits $CS_{bio,k,h}$ are calculated based on the amount of stored biogenic carbon dioxide $\dot{S}_{bCO_2,k,h}$, as

$$CS_{bio,k,h} = \dot{S}_{bCO_2,k,h} \ \forall (k,h) \in \mathcal{T}. \tag{47}$$

4. Results and discussion

In the following, we first analyze the optimal design of the concrete production process under steady-state operation (Sections 4.2 and 4.3) for different scenarios. Then, we perform integrated design and operation of a flexible plant, and assess the potential total annualized costs savings and shifted electricity demand (Section 4.4).

4.1. Scenario definition

In our previous work (Ojeda-Paredes et al., 2025), we showed that optimal designs for reducing carbon emissions in Ordinary Portland cement production strongly depend on local conditions. In the present study, we adopt a similar perspective and define scenarios based on two crucial parameters, namely (i) the availability of biomass and (ii) the emission factor of the utilized electricity mix. Biomass is represented by wood chips with a cost of 95.06 EUR/t (C.A.R.M.E.N. e.V., 2024) and an upstream emission factor of 23.6 kg $CO_{2_{eq}}$/t (Yang et al., 2022). In the biomass availability scenario, biomass is assumed to be a feasible local fuel option for the plant. This represents a case in which the required wood chips can be sourced locally without prohibitive costs or major sustainability constraints, in line with reported restrictions for biomass use in cement manufacturing, including pre-treatment requirements, local resource availability, transport costs, and sustainable sourcing (International Energy Agency (IEA) Bioenergy, 2021). In contrast, the biomass unavailability scenario reflects conditions in which these requirements are not met, including competing biomass uses such as food/feed, materials, and other energy applications (International Energy Agency (IEA) Bioenergy, 2008; Mignogna et al., 2024). When biomass is unavailable, the fuel set is restricted to natural gas and hydrogen, the latter being either market-sourced or produced on-site. For the electricity mix, we consider two greenhouse-gas intensities: (i) a high-GWI case based on Germany in 2024 (363 g $CO_{2_{eq}}$/kWh Icha and Lauf, 2025), and (ii) a low-GWI case corresponding to Norway in 2022 (10 g $CO_{2_{eq}}$/kWh International Energy Agency (IEA), 2022). These parameters result in four scenarios, namely high-GWI with and without biomass and low-GWI with and without biomass.

4.2. Optimal design for the steady-state operation: High-GWI electricity mix

Fig. 3 shows the Pareto fronts for the high-GWI scenarios, considering both availability and unavailability of biomass. Each marker on the front represents a Pareto-optimal design defined by its cement composition (ratio of Portland cement and recycled belite cement clinker, RC-BCC), raw meal composition, and kiln energy source. Interpolated lines between the optimal designs are added to guide the eye of the reader. In bi-objective optimization, Pareto optimality implies that no objective can be improved without worsening the other. In total, five Pareto-optimal designs are computed for each scenario with respect to the two objective functions, i.e., the total annualized cost (TAC) and the global warming impact (GWI).

The nonlinear shape of the Pareto fronts reflects the fact that the trade-offs between cost and emissions are technology and material dependent. In both scenarios (biomass availability and no biomass availability), the cost-optimal design corresponds to the reference configuration, i.e., concrete is produced exclusively with Portland cement and no additional units for RC-BCC production or CO_2 capture are installed (Reference in Fig. 3). Optimal GWI reductions can be achieved via three process configurations: (i) the electric rotary kiln with increasing RC-BCC substitution (second Pareto solution from the left), (ii) the oxyfuel-fired rotary kiln using non-biogenic fuels and with increasing use of RC-BCC in the concrete production (third to fifth Pareto solutions from the left in the unavailability of biomass case), and (iii) the oxyfuel-fired rotary kiln using natural gas or biomass as fuels and with increasing use of RC-BCC in the concrete production (third to fifth Pareto solutions from the left in the availability of biomass case), as shown in Fig. 3.

When RC-BCC is produced, CO_2 from fuel combustion (natural gas or biomass) and limestone calcination is captured and utilized to produce carbonated aggregates. For the Pareto-optimal designs that reduce GWI, the optimizer selects the aqueous mineral carbonation over the dry gas–solid route. This selection is determined mainly by (i) the energy requirements and (ii) the capital costs of the auxiliary equipment. The aqueous route requires energy for solid–liquid separation

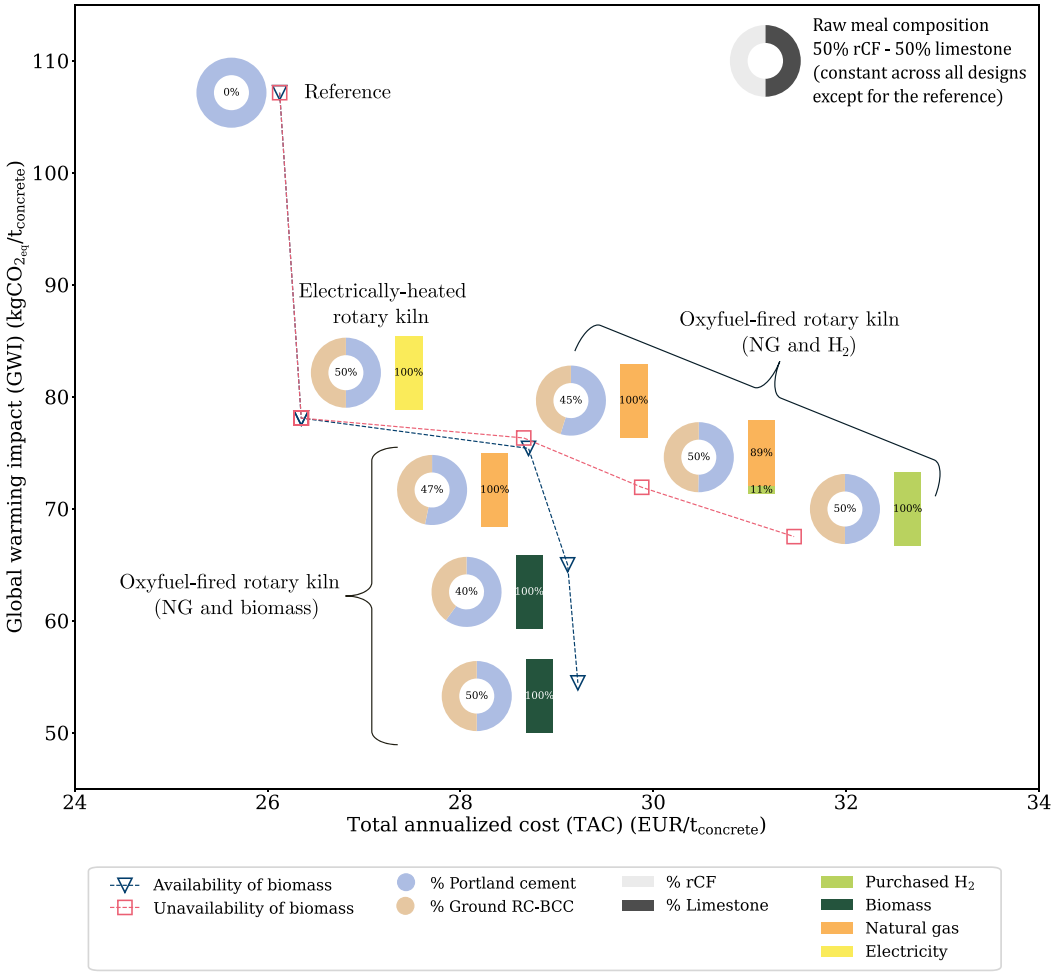

Fig. 3. Pareto fronts for high-GWI scenarios considering both availability (blue triangles) and unavailability (red squares) of biomass. For each Pareto-optimal design, circular and bar plots are displayed. The circles indicate the share of Portland cement (light blue) and recycled belite cement clinker (RC-BCC, beige) within the cement fraction of concrete, with the RC-BCC percentage shown at the center. The vertical bars denote the selected kiln energy source, i.e., electricity (yellow), biomass (dark green), natural gas (orange), or purchased hydrogen (light green), with values indicating the respective share of each energy source supplying the kiln.

and for drying the carbonated aggregates (assumed electric heating, see Fig. 1), whereas the dry route requires heat to raise the temperature in the carbonation reactor (assumed to be supplied by an external electric boiler, see Fig. 1), which increases CAPEX. However, we emphasize that this result is sensitive to the cost and energy parameters considered for both routes, and different conditions (e.g., availability of waste heat) could make the dry route more competitive.

In the electrically-heated rotary kiln configuration, a 50% RC-BCC replacement lowers GWI by 27.1% relative to the reference, while TAC increases only slightly from 26.1 to 26.3 EUR/t concrete. The oxyfuel-fired rotary kiln configuration enables the deepest decarbonization potential. If biomass is available, it is both economically and environmentally preferred over hydrogen or natural gas. The largest GWI reduction (49.2%) is achieved by using biomass in the oxyfuel-fired rotary kiln, due to credits from converting biogenic CO_2 into stable solids (long-term CO_2 storage), at a TAC of 29.2 EUR/t concrete. If biomass is not available, market-sourced hydrogen becomes the preferred fuel, leading to a 37% GWI reduction relative to the reference, but at a higher cost of 31.5 EUR/t concrete. Hence, a combination of carbon-neutral fuels (biomass and green hydrogen) and high RC-BCC substitution rates is crucial to achieve strong GWI reductions.

Across all Pareto-optimal designs, except for the reference, the recycled concrete fines (rCF) share remains at the upper bound of 50%, with the remaining 50% corresponding to limestone. This outcome results from the modeling assumptions, i.e., rCF is obtained from waste concrete and considered as cost and emission free, whereas limestone must be purchased and therefore involves both cost and GWI. Hence, the optimizer consistently selects the maximum rCF share. This is in contrast to the cement composition (Portland cement and RC-BCC), where intermediate substitution levels are obtained along the Pareto front.

Interestingly, at the third Pareto solution (first oxyfuel-fired rotary kiln design), the optimizer selects a higher share of Portland cement compared to the lowest-GWI electrically-heated rotary kiln solution. This raises upstream emissions, but the effect is partly offset by avoided emissions from electric heating. Consequently, GWI remains comparable to the electrically-heated rotary kiln case, despite a significantly higher TAC. At the fifth Pareto solution, increasing RC-BCC substitution again reduces GWI. Fuel choice then becomes decisive, natural gas leads to persistent fossil emissions, hydrogen reduces them at higher cost, while biomass provides the lowest-GWI designs that are also cheaper.

Although electric heating has been proposed as a decarbonization strategy for cement kilns (Pisciotta et al., 2022), its potential is strongly constrained by the carbon intensity of the electricity mix. Here, under the high-GWI electricity mix, indirect emissions largely offset the potential benefits of electrification.

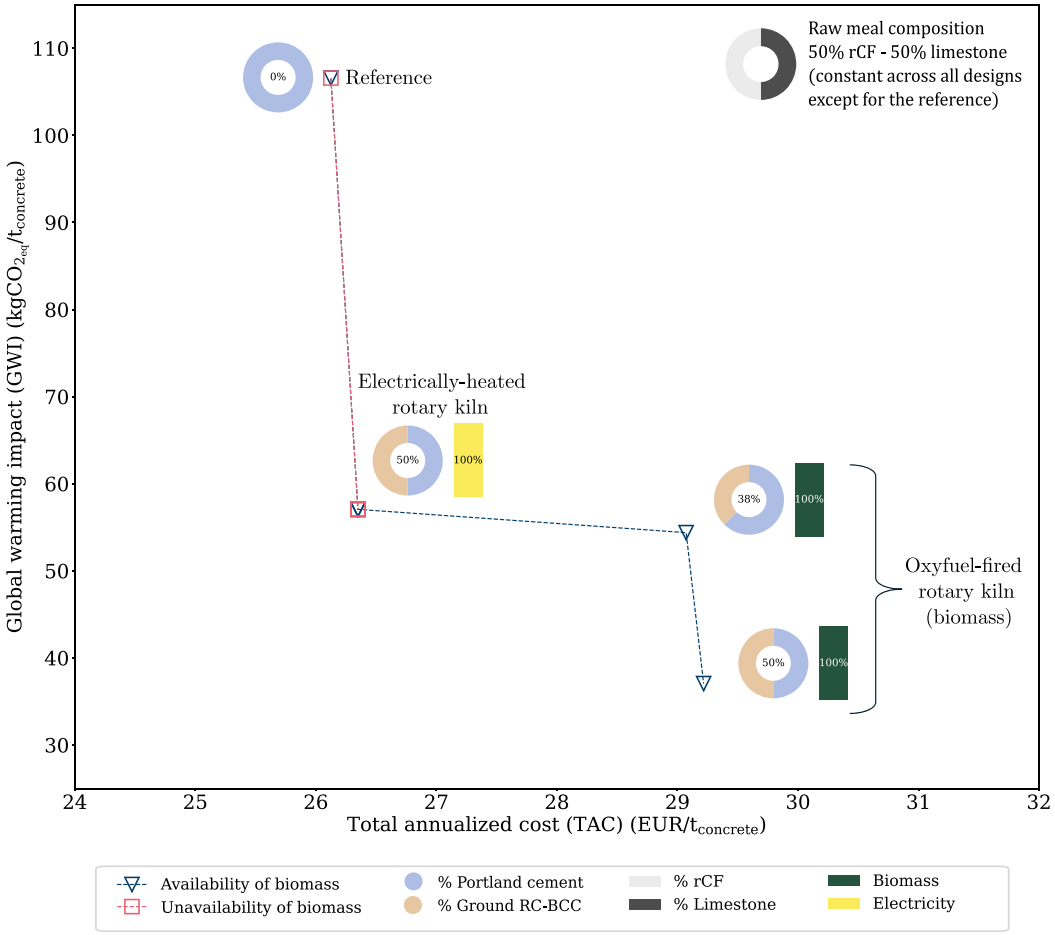

Fig. 4. Pareto fronts for low-GWI scenarios considering both availability (blue triangles) and unavailability (red squares) of biomass. For each Pareto-optimal design, circular and bar plots are displayed. The circles indicate the share of Portland cement (light blue) and recycled belite cement clinker (RC-BCC, beige) within the cement fraction of concrete, with the RC-BCC percentage shown at the center. The vertical bars denote the selected kiln energy source, i.e., electricity (yellow) and biomass (dark green), with values indicating the respective share of each energy source supplying the kiln (100% in both cases).

4.3. Optimal design for the steady-state operation: Low-GWI electricity mix

At a carbon intensity of 10 g $CO_{2_{eq}}$/kWh, the Pareto fronts shrink considerably compared to the high-GWI case (see Fig. 4). Although we considered five equidistant GWI values when we executed the augmented ϵ−constrained method (Mavrotas, 2009), only four Pareto-optimal designs remain for the scenario with biomass availability and two for the scenario without biomass. Accordingly, only two process configurations are optimal for reducing GWI, namely (i) the electric rotary kiln and (ii) the oxyfuel-fired rotary kiln with biomass. For the oxyfuel-fired rotary kiln configuration, natural gas is excluded by the optimizer due to its high fossil emissions, while hydrogen is not selected because electrification is more cost effective for reducing GWI. Compared to the high-GWI case, this shows that a more decarbonized electricity mix leads to different optimal solutions, both in terms of process configurations and fuel choices.

When biomass is not available, switching from the reference design (100% Portland cement) to the electrically-heated rotary kiln with 50% RC-BCC substitution raises TAC by only 0.9% (from 26.1 to 26.3 EUR/t concrete), while reducing GWI by 46.5%. This value is 29.9% lower than the corresponding design in the high-GWI case (cf. Fig. 3), illustrating the strong competitiveness of electrification under a low-carbon electricity mix.

The oxyfuel-fired rotary kiln with biomass achieves the lowest GWI, 37.1 kg $CO_{2_{eq}}$/t concrete. Compared to the minimum-GWI design with biomass in the high-electricity-GWI case, this corresponds to a 32% lower value, since electricity-driven units such as the air separation and carbon purification benefit directly from the cleaner mix. This reflects that a low-GWI electricity mix improves the environmental performance of both the electrically-heated rotary kiln and the oxyfuel-fired rotary kiln with biomass.

Since the carbon intensity of the electricity mix in many countries is expected to decrease due to the rise of renewables (International Energy Agency (IEA), 2021), the Pareto-optimal designs under the low-GWI case are considered more representative of future conditions. Therefore, their electricity consumption and cost structures are analyzed in detail in the following subsections.

4.3.1. Electricity consumption of Pareto-optimal designs

Fig. 5 shows the electricity demand of the electricity-driven process units across the Pareto-optimal designs under a low-GWI electricity mix. For the minimum-TAC design (1), electricity demand is limited to the concrete production section, with 0.18 MW in both scenarios (biomass availability and non-availability).

At the minimum-GWI design without biomass availability (2), the total electricity demand amounts to 6.9 MW, equivalent to 60 kWh/t concrete. The electrically-heated rotary kiln is the largest contributor (3.8 MW, 56% of the total), followed by the aqueous separation section (filtration and drying, 1.5 MW). Raw material pretreatment (crushing, drying, and milling) and clinker milling together account for 0.98 MW. In contrast, with biomass availability the total electricity demand, i.e., 5.7 MW (49.3 kWh/t concrete), is lower than that in

the electrically-heated rotary kiln configuration, for a minimal-GWI (4), while the distribution across units changes markedly. The aqueous separation section dominates (3.3 MW, 57.7% of the total), whereas the air separation and carbon purification units together add 1.1 MW. As detailed in Section 2.1, we assume electric preheating provided that the electric rotary kiln is selected by the optimizer, leading to an additional electricity consumption of 0.4 MW attributed to the preheating stage (2).

Overall, the lowest-GWI designs in both scenarios (biomass availability and non-availability) correspond to the highest electricity consumption. However, their electricity demand distribution differ substantially. When biomass is not available, electricity is mainly consumed by the kiln and the aqueous separation, whereas with biomass, electricity consumption is distributed across several units, including aqueous separation, air separation, and carbon purification.

4.3.2. Cost breakdown of Pareto-optimal designs

Fig. 6 shows the cost distribution of the total annualized cost (TAC) for the Pareto-optimal designs under a low-GWI electricity mix (cf. Fig. 4), including the contributions of operational expenditures (OPEX) and capital expenditures (CAPEX).

Overall, OPEX dominate across all designs, regardless of biomass availability, kiln configuration, or the degree of Portland cement replacement by RC-BCC. At the minimum-TAC design, OPEX arise almost entirely from concrete constituents (25.9 EUR/t concrete, 99.5% of OPEX), with electricity contributing less than 1%. Besides, CAPEX are negligible (0.3% of TAC), as concrete production involves only batching and mixing operations. When Portland cement is partially replaced by 50% RC-BCC, electricity costs increase significantly, to 4.7 EUR/t (second Pareto-solution) or to 3.9 EUR/t (fourth Pareto-solution), depending on the kiln configuration. This increase reflects the electricity-intensive production of RC-BCC, which involves the kiln (electric), CO_2 capture, and aqueous carbonation. Furthermore, in the oxyfuel-fired rotary kiln configuration (fourth Pareto solution), the production of RC-BCC decreases aggregate costs by 1.1 EUR/t concrete due to the on-site production of carbonated aggregates.

For the scenario with biomass, substituting Portland cement with RC-BCC leads to CAPEX values between 4.3 and 7.2 EUR/t concrete (second and fourth Pareto-solutions respectively), as a result of the installation of technologies for RC-BCC and aggregate production. The rotary kiln accounts for approximately 68.2% and 31% of the CAPEX in the electrically-heated and oxyfuel-fired kiln configurations, respectively. In the latter case, additional units are required, such as the air separation unit and carbon purification unit, which together account for about 43.9% of the investment cost.

Additionally, replacing Portland cement with RC-BCC reshapes the cost structure, i.e., the economic burden is shifted from conventional materials to electricity and capital-intensive technologies. As a result, costs associated with Portland cement and aggregates decrease, while electricity expenditures and capital investment increase. Furthermore, for the oxyfuel-fired rotary kiln configuration, additional costs arise from biomass purchase and CO_2 certificates, further contributing to the total annualized cost (TAC). The payment for CO_2 certificates arises from the uncaptured fraction of CO_2 from limestone calcination, due to the assumed 90% capture rate in the carbon purification unit.

4.3.3. Impact of increasing RC-BCC substitution above 50%

The Pareto fronts in Figs. 3 and 4 show that increasing the substitution levels of RC-BCC significantly decreases the GWI. Based on reported substitution levels at laboratory scale (Stemmermann et al., 2022), we assume a maximum substitution of 50%. Here, we compute optimal designs with fixed substitution levels ranging from 60 to 100% of RC-BCC, see Fig. 7, assuming that higher substitution ratios might be feasible depending on client specifications and technical standards for concrete production.

Higher replacement rates of RC-BCC would further decrease the GWI, leading to very low values in the electrically-heated rotary kiln configuration (7.5 kg $CO_{2_{eq}}$/t concrete at 100% substitution) and negative values in the oxyfuel-fired rotary kiln configuration (−32.5 kg $CO_{2eq}/t_{concrete}$ at 100%). In the oxyfuel-fired rotary kiln configuration, negative GWI values are already achieved at 80% substitution (−4.7 kg $CO_{2_{eq}}$/t concrete).

Higher substitution levels of RC-BCC can also be economically preferable. This outcome can be partly explained by the fact that most of the TAC arises from OPEX (cf. Fig. 6); in particular, mainly the TAC can be attributed to the purchase of concrete constituents (aggregates and Portland cement), which decrease with the on-site production of RC-BCC and aggregates. In contrast, for the electrically-heated rotary kiln, substitution levels of 60% and more would be more cost-effective than the reference configuration (100% Portland cement). However, the electrically-heated rotary kiln configuration is very sensitive to electricity prices. For instance, at 100% RC-BCC, electricity accounts for 51% of OPEX and 37.4% of TAC. Hence, electricity prices above the price considered in this analysis (78.51 EUR/MWh for 2024 Bundesnetzagentur|SMARD.de, 2024) could offset the apparent TAC reduction relative to the 100% Portland cement reference.

4.4. Integrated design and operation

In the following, we assess the benefits of integrating design and operation. Specifically, we quantify the potential cost savings considering varying electricity prices and evaluate the demand response potential of low-carbon concrete production. Further, we analyze the optimal capacities of selected technologies and storage units. To account for the effect of temporal aggregation, the quasi-stationary model is solved for different numbers of clusters, i.e., $K = 4, 6, 8, 10, 12, 14, 16, 18$, and 20. Accordingly, the results in this section are reported as ranges over the investigated values of K.

As a basis, we use the GWI-optimal designs for steady-state operation from the low-GWI scenarios with and without biomass availability (Section 4.3). We fix the kiln configuration (electrically-heated rotary kiln and oxyfuel-fired rotary kiln with biomass) and the material composition (50% RC-BCC and 50% recycled concrete fines), and then minimize TAC. Compared to the corresponding steady-state reference designs, the discrete-time quasi-stationary formulation enables time-dependent operation under varying electricity prices, thereby capturing load shifting behavior that cannot be represented in a steady-state formulation.

Table 3 reports the resulting TAC reductions, annual electricity savings, load shifting, and wall time, where the latter refers to the wall-clock time elapsed during solution of the problem by the Gurobi solver. Flexible operation, i.e., the ability of the process to operate under different operating conditions (Swaney and Grossmann, 1985; Luo et al., 2022), leads to negligible TAC reductions compared to the steady-state reference. The TAC reduction ranges from 0.04% to 0.46% for the electrically-heated rotary kiln-based process and from 0.09% to 0.33% for the oxyfuel-fired rotary kiln-based process with biomass. In contrast, the effect on the electricity costs is more pronounced. Annual electricity costs decrease by 2.2–2.8% (84–108 kEUR) for the electrically-heated rotary kiln and by 13.4–18.2% (428–582 kEUR) for the oxyfuel-fired rotary kiln. The limited TAC reductions are due to the additional requirements of the flexible operation, i.e., the installation of storage units, auxiliary units (e.g., CO_2 compressor), as well as the oversizing of certain process units (e.g., the mills). These investments lead to higher annualized CAPEX compared to the steady-state reference, ranging from approximately 54–99 kEUR (+1.5–+2.8%) for the electrically-heated rotary kiln and 398–502 kEUR (+6.7–+8.4%) for the oxyfuel-fired rotary kiln.

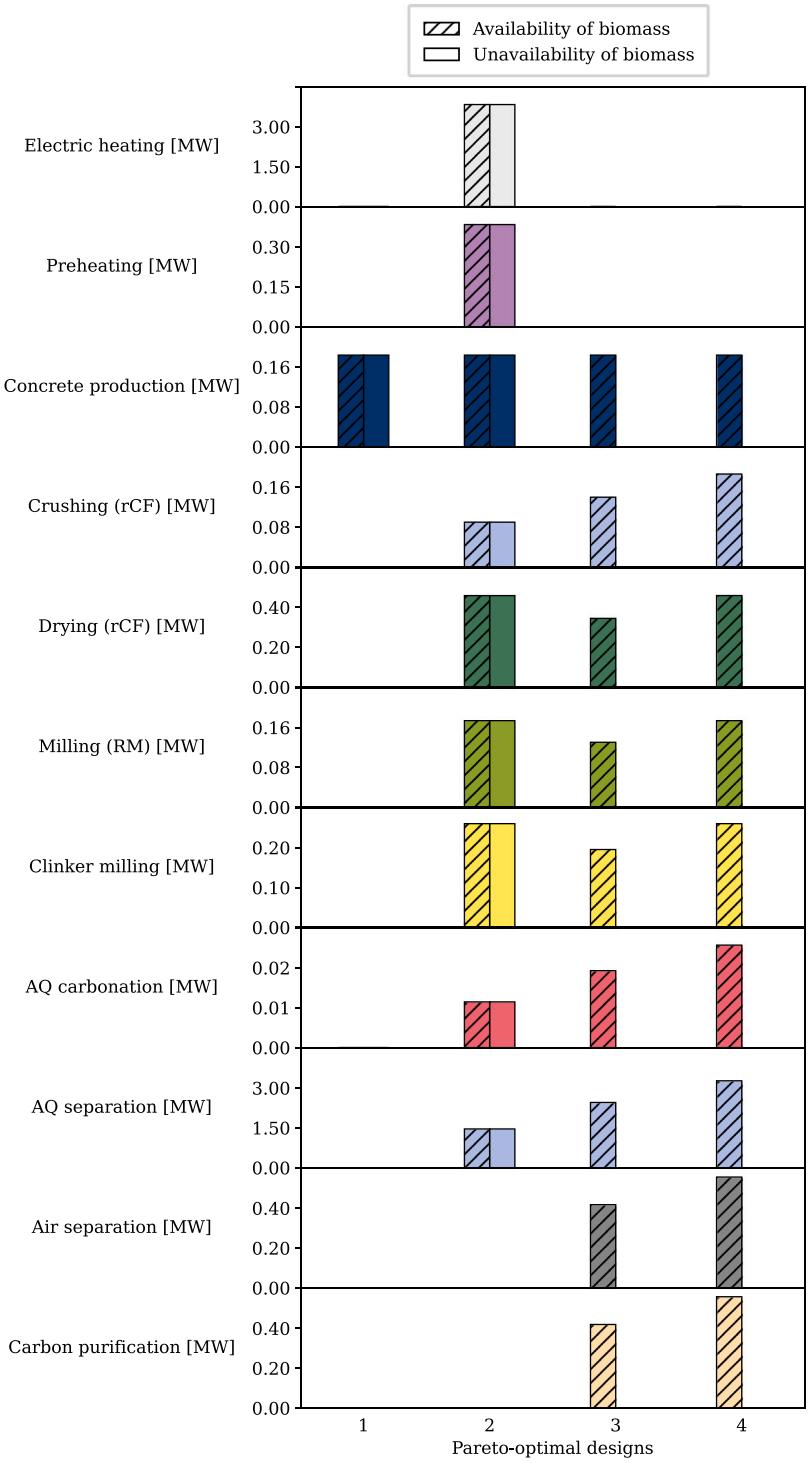

Fig. 5. Electricity demand of process units across Pareto-optimal designs considering a low-GWI electricity mix. Results are shown for scenarios with biomass availability (hatched bars) and without biomass availability (plain bars).

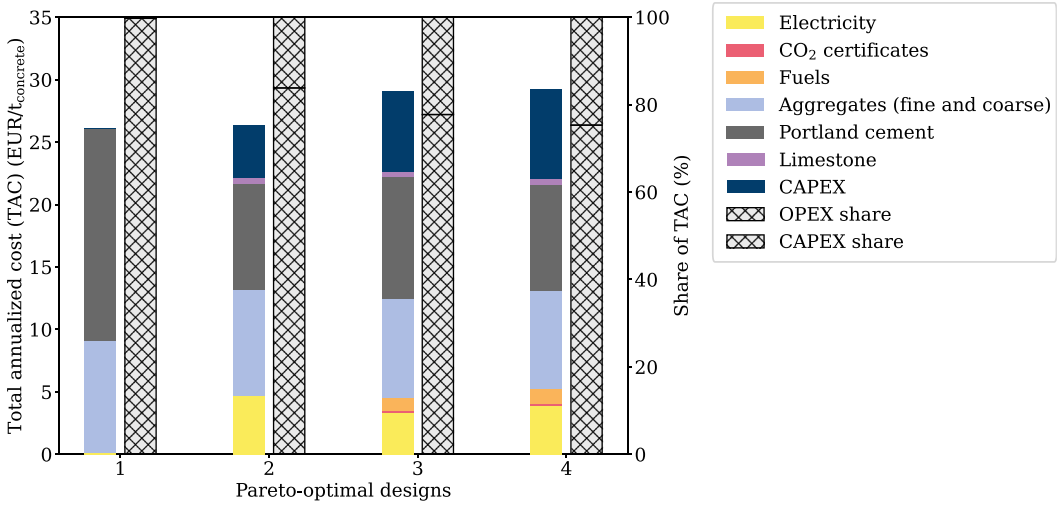

Fig. 6. TAC breakdown for Pareto-optimal designs in Fig. 4: The stacked first bars show operational costs, including expenses for electricity, CO_2 certificates, fuels (biomass), aggregates (fine and coarse), Portland cement and limestone. The second stacked bars show the share of operational expenditures (OPEX) and capital expenditures (CAPEX).

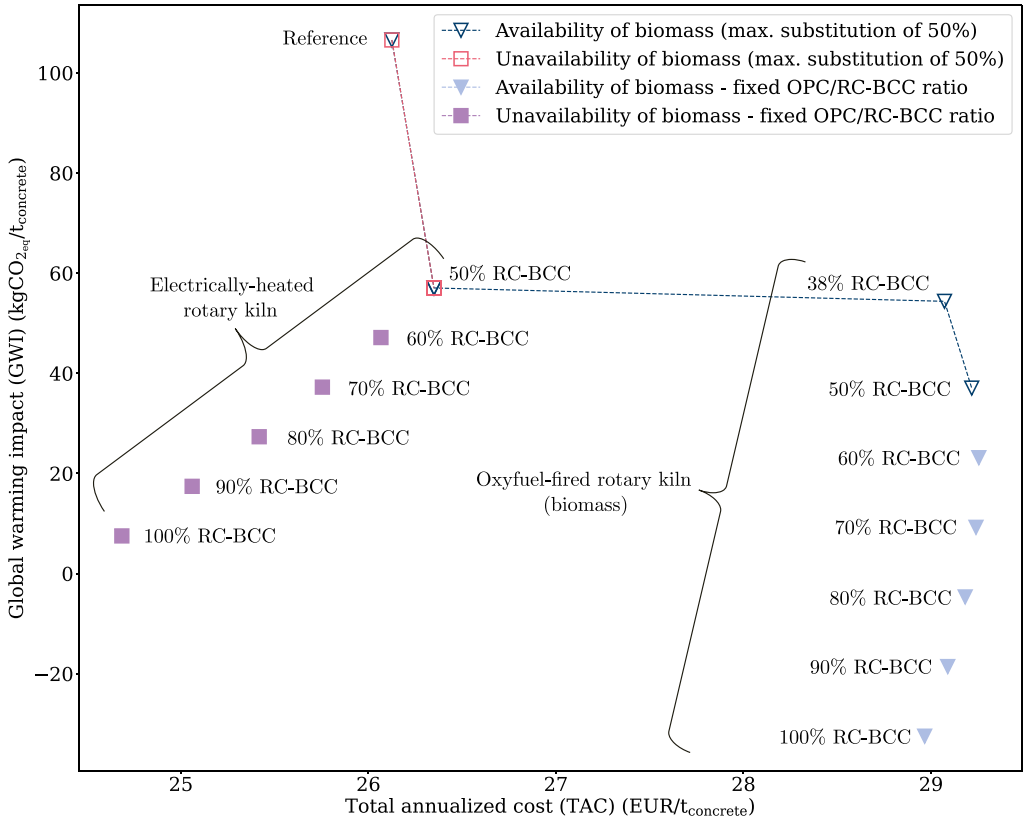

Fig. 7. Pareto fronts for low-GWI scenarios considering both availability (blue triangles) and unavailability (red squares) of biomass. Optimal solutions under fixed substitution levels of RC-BCC (60%–100%) are represented by purple squares (availability of biomass) and light blue triangles (unavailability of biomass).

Previous studies on demand side management in cement plants report electricity costs savings ranging from 4% to 14% (Summerbell et al., 2017; Mossie et al., 2025; Rojas-Innocenti et al., 2024). The electricity cost savings obtained for the oxyfuel-fired rotary kiln, 13.4–18.2%, are therefore within or slightly above the range reported in the literature, depending on the temporal aggregation. Savings from the electrically-heated rotary kiln case are comparatively lower, as fewer flexible units are activated in the optimal design. Specifically,

Table 3
TAC reduction, annual electricity savings, load shifting, and wall time for $K = 4, 6, 8, 10, 12, 14, 16, 18,$ and 20 representative-day clusters for (a) the electrically-heated rotary kiln-based process and (b) the oxyfuel-fired rotary kiln-based process with biomass.

(a) Electric kiln				
Clusters	TAC reductions (%)	Electricity savings (%)	Load shifting (%)	Wall time (s)
4	0.46	2.79	3.7	47
6	0.08	2.16	4.2	55
8	0.11	2.64	4.5	178
10	0.08	2.62	4.7	543
12	0.14	2.52	4.2	978
14	0.08	2.28	4.3	1421
16	0.04	2.77	5.3	1777
18	0.09	2.34	4.4	2149
20	0.09	2.37	4.5	3677
(b) Oxyfuel kiln				
Clusters	TAC reductions (%)	Electricity savings (%)	Load shifting (%)	Wall time (s)
4	0.31	13.82	26.2	161
6	0.12	13.37	25.0	195
8	0.18	14.39	25.7	522
10	0.11	16.12	28.9	1339
12	0.09	17.23	30.5	1973
14	0.22	17.25	30.6	2736
16	0.12	16.70	29.3	3626
18	0.28	17.76	30.4	4391
20	0.33	18.17	30.3	6436

only units in the cement production line, i.e., crusher, dryer, raw mill, and clinker mill, contribute to flexibility. This can be attributed to two main factors. First, we assume day-ahead electricity prices, whereas other studies consider different market frameworks, such as spot prices (Summerbell et al., 2017) or time-of-use tariffs (Mossie et al., 2025), which can exhibit higher or lower price variability, respectively. As shown by Rojas-Innocenti et al. (2024), demand response potential is highly sensitive to market-specific conditions and seasonal fluctuations. Second, our model integrates design and operation, and accounts for total annualized costs (TAC), which limits the oversizing of electricity-driven units and the sizing of storage units. In contrast, most studies focus solely on operational scheduling under a fixed process design, and typically report electricity cost savings without considering capital investments. Our results thus highlight the importance of accounting for investment costs required to enable flexibility. Including additional electricity markets, such as intraday or reserve capacity markets, might lead to further savings and enhance the demand response potential. Moreover, higher price volatility on the day-ahead market could increase the economic benefit of flexibility.

Fig. 8 illustrates the operational response of the two process configurations for one representative day. The example corresponds to $K = 6$, cluster 1, which has a probability of occurrence of 34.7% (cf. Fig. 2). The figure shows how electricity consumption is shifted to hours with lower electricity prices. In both process configurations, the rotary kiln operates continuously, as we assume no flexibility in that unit operation. The continuous operation restricts the electricity-driven upstream and downstream units that are directly coupled to the kiln, such as the preheater (PRE) in the electrically-heated rotary kiln case and the carbon purification unit (CPU) in the oxyfuel-fired rotary kiln configuration, which remain at steady load. Thus, demand response within the RC-BCC production line is mainly attributed to the raw meal pretreatment (crushing, drying and milling) and clinker milling sections. Notably, the operating schedules of the drying, raw milling, and clinker milling tasks are similar in both kiln configurations, typically operating at full capacity during periods with more favorable electricity prices. In contrast, the crusher operation profile is different for the two process configurations. In the oxyfuel-fired rotary kiln-based process, the crusher operation is limited by dependencies with the aqueous mineral carbonation section (AQ-CARB and AQ-SEP), resulting in periods of lower electricity consumption or shutdown when the carbonation process is not operating. The finding that milling operations are the primary contributors to demand response in cement plants aligns with previous studies (Estelmann et al., 2018; Mossie et al., 2025).

Overall, both kiln configurations allow demand response, although the oxyfuel-fired rotary kiln process offers greater operational flexibility than the electrically-heated rotary kiln process. In the oxyfuel-fired rotary kiln process, the aqueous mineral carbonation task (i.e., carbonation and drying) decreases its electricity demand or is shut down during hours of high electricity prices, whereas such load shifting is not economically viable in the electrically-heated rotary kiln process. This can be partly explained by the fact that enabling flexibility in the aqueous separation process requires additional units such as a CO_2 storage tank and compressor, which increase CAPEX which cannot be fully offset by electricity savings in the electrically-heated rotary kiln configuration. Moreover, CO_2 from limestone calcination in the electrically-heated rotary kiln is released at atmospheric pressure (1.01 bar), and compressing it to the storage pressure (25 bar) implies a higher electricity demand compared to the oxyfuel-fired rotary kiln case, where CO_2 is already available at 16.5 bar from the carbon purification unit (CPU). Detailed calculations of the electricity demand for CO_2 compression can be found in Section 3 and Tab. 6 of the supporting materials. The annual shifted electricity demand ranges from 3.7% to 5.3% (1.8 GWh to 2.6 GWh), for the electrically-heated rotary kiln process and from 25.0% to 30.6% (10.3 GWh to 12.6 GWh) for the oxyfuel-fired rotary kiln process, relative to their respective annual electricity consumption (see Table 3). This significant difference demonstrates that flexibility in concrete production can also be achieved from carbon capture and utilization (CCU) units. Specifically, the aqueous mineral carbonation section (AQ-CARB and AQ-SEP) shifts approximately 35–45% of its electricity consumption across the tested temporal aggregations of electricity price data.

As load shifting is achieved by (i) implementing intermediate storage units and (ii) oversizing of selected process units, Fig. 9 compares the optimal installed capacities of flexible unit operations with the corresponding steady-state capacities. The figure reports both the mean capacity over the tested values of K and the corresponding min–max range.

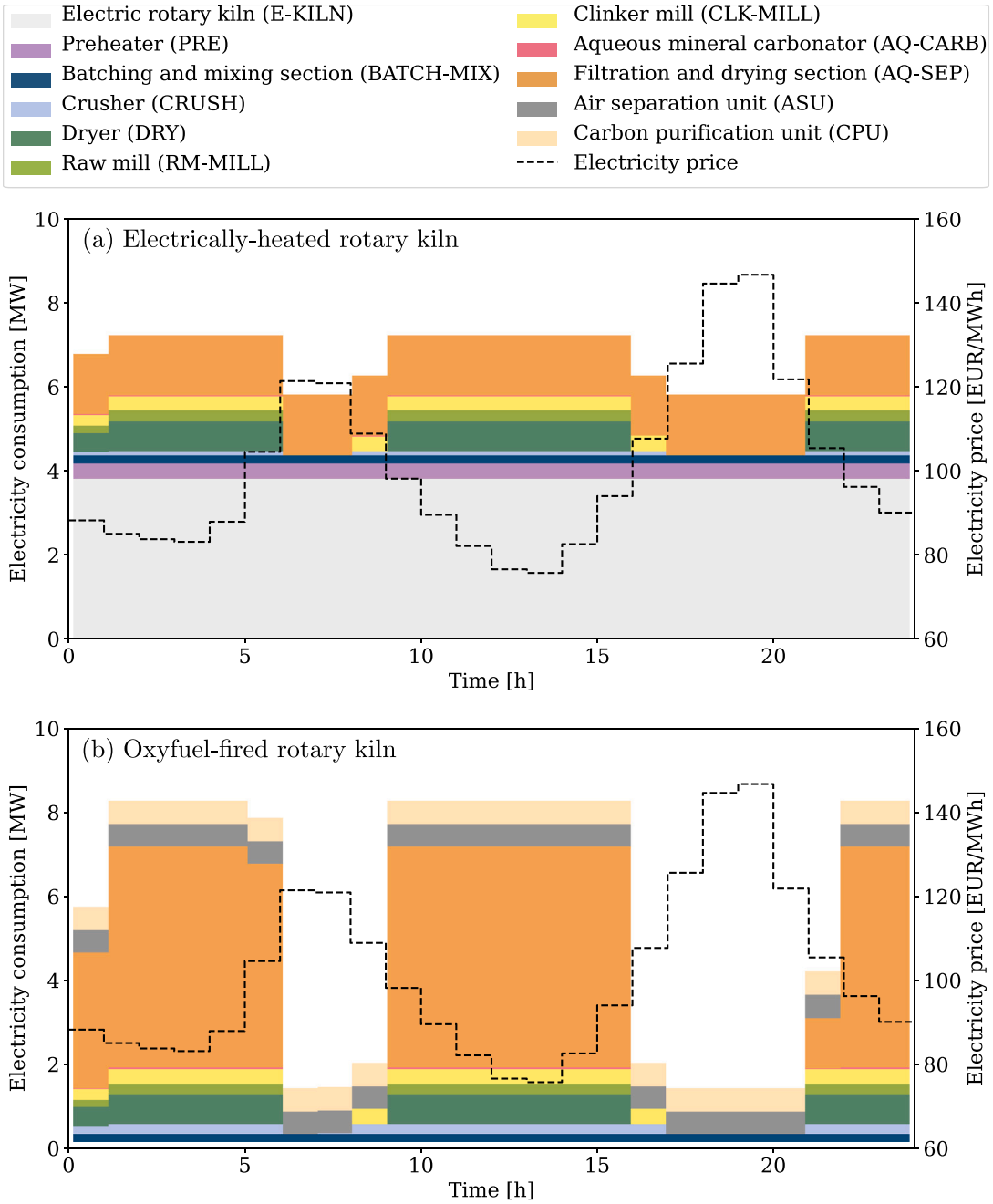

Fig. 8. Electricity consumption of concrete production considering 50% of RC-BCC for (a) the electrically-heated rotary kiln and the (b) oxyfuel-fired rotary kiln with biomass. Shown is an illustrative demand response schedule for $K = 6$, considering the first typical day (cluster 1), which has a probability of occurrence of 34.7% (cf. Fig. 2).

Overall, the variation in unit capacities across the tested values of K is moderate compared with the difference between the steady-state and flexible designs. This indicates that the optimal sizing of the main flexible units is relatively robust with respect to the temporal aggregation. In the electrically-heated rotary kiln configuration, the largest absolute increase is observed for the dryer, whose capacity ranges from 0.66 to 0.88 MW, compared to 0.46 MW in the steady-state design. In the oxyfuel-fired rotary kiln, due to the electricity demand required for drying the carbonated material, the aqueous separation section (AQ-SEP) shows the largest capacity increase, ranging from 5.31 to 6.27 MW compared to 3.27 MW in the steady-state design. This reflects the role of CCU-related units in providing demand response.

Fig. 10 shows the corresponding annualized CAPEX of the flexible units and the corresponding units of the steady-state designs. For the electrically-heated rotary kiln configuration, the CAPEX increments of individual flexible units remain moderate, with the largest increments associated with the raw mill and dryer. Across the tested values of K, the annualized CAPEX increment of the raw mill ranges from 23 to 46 kEUR, while that of the dryer ranges from 15 to 30 kEUR. For the oxyfuel-fired rotary kiln configuration, the largest annualized CAPEX increments are associated with the CCU-related units. The annualized CAPEX increment of the aqueous mineral carbonator ranges from 168 to 237 kEUR, while that of the filtration and drying section ranges from 106 to 150 kEUR. Thus, although CCU units increase the flexibility potential, they also introduce a significant additional investment requirement. As a result, despite significant electricity cost savings, the TAC reduction remains small.

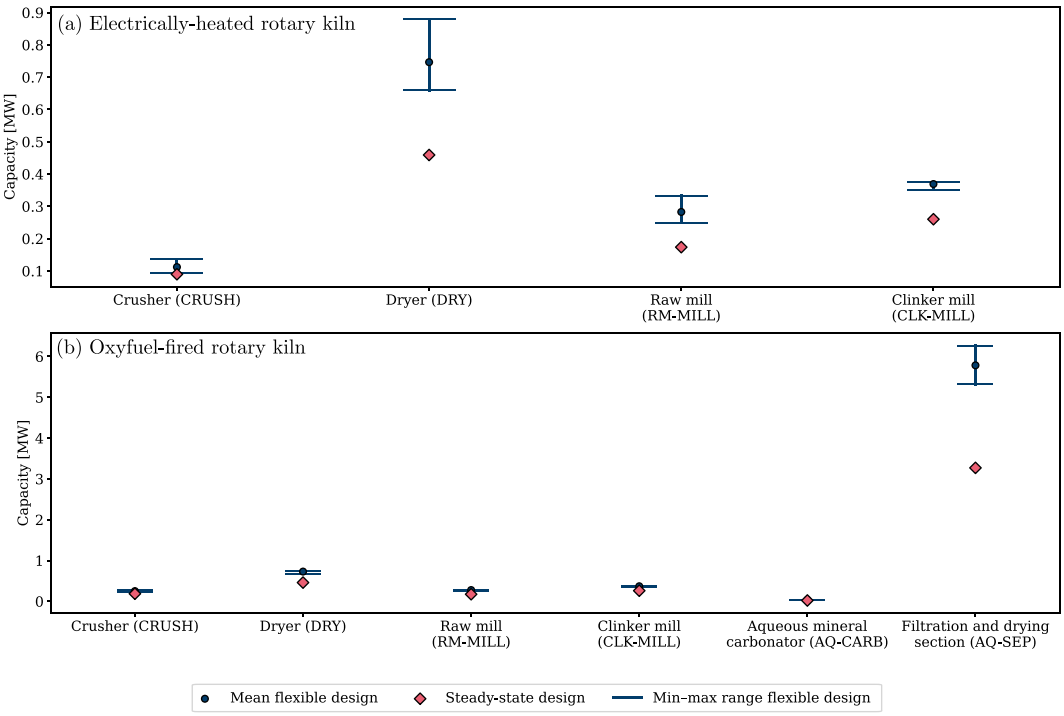

Fig. 9. Optimal capacities of flexible unit operations compared to the corresponding steady-state configuration for $K = 4, 6, 8, 10, 12, 14, 16, 18$, and 20 for (a) the electrically-heated rotary kiln-based process and (b) the oxyfuel-fired rotary kiln-based process with biomass. Markers indicate the mean capacities over the tested values of K, and bars indicate the corresponding min–max ranges.

As described previously, the total annualized CAPEX increase ranges from 54 to 99 kEUR for the electrically-heated rotary kiln and from 398 to 502 kEUR for the oxyfuel-fired rotary kiln. In both kiln configurations, these increases are primarily driven by equipment oversizing rather than the implementation of storage units or auxiliary equipment. In particular, in the electrically-heated rotary kiln configuration, oversizing ranges from 96.8% to 97.3% of the total CAPEX increase. In the oxyfuel-fired rotary kiln configuration, it accounts for about 85.1–86.4%, with the remainder attributed to storage units and the CO_2 compressor. These results demonstrate that enabling operational flexibility through oversizing leads to significant additional investment cost, not only for capital intensive CCU units, but also for RC-BCC production units, even if their individual CAPEX contributions are moderate. Consequently, oversizing costs can limit the flexibility potential, as the trade-off between investment and electricity cost savings varies significantly across process units.

Table 4 reports the storage capacities obtained for the different numbers of clusters. No clear trend but, depending on the stored material, significant variations can be observed. Thus, the optimal storage sizes are quite sensitive with respect to the particular representative price profiles generated by the clustering, which can be explained by the relatively low CAPEX of storage.

All storage units are considered as intermediate buffers, which are filled and emptied according to the varying operation of upstream and downstream process units. In particular, bulk solid materials such as recycled aggregates and carbonated aggregates are assumed to be stored in open stockpiles, whereas recycled concrete fines, raw meal, clinker, and ground RC-BCC are assumed to require enclosed storage (e.g., silos or sheds). Pressurized tanks are considered for the storage of O_2 and CO_2. Larger storage capacities enable decoupling between process sections and allow temporary shutdowns during periods of high electricity prices, whereas smaller storage capacities restrict this flexibility. The largest storage capacities are obtained for recycled aggregates. In the electrically-heated rotary kiln configuration, recycled aggregate storage ranges from 50 to 224.5 t, while in the oxyfuel-fired rotary kiln configuration it ranges from 225.4 to 557.7 t. In contrast, the capacities of clinker and ground RC-BCC storage vary within a narrower range, approximately 47.8–65.5 t for both kiln configurations.

Surprisingly, across all tested temporal aggregations, O_2 storage is not selected by the optimizer to provide flexibility in the oxyfuel-fired rotary kiln configuration. We attribute this result to the fact that storing O_2 would lead to additional CAPEX, due to the compressor and the storage tank, and oversizing of the air separation unit (ASU). In the steady-state operation, the ASU already represents the second most capital-intensive unit after the rotary kiln, accounting for approximately 25% of the total CAPEX.

5. Conclusion

We determined the optimal design of a low-carbon concrete production plant under varying material composition and capable of adjusting its electricity consumption under time-varying electricity prices. The plant integrates a novel recycled belite cement clinker (RC-BCC) process. To this end, we formulated an integrated design and scheduling model that includes both design decisions (e.g., technology selection) and operational decisions (e.g., mass flows), and evaluated scenarios defined by availability of biomass and the emission factor of the electricity mix.

The results demonstrate that replacing Portland cement with RC-BCC produced via either an electrically-heated or an oxyfuel-fired rotary kiln, combined with aqueous mineral carbonation, can significantly reduce the global warming impact (GWI). At a substitution level

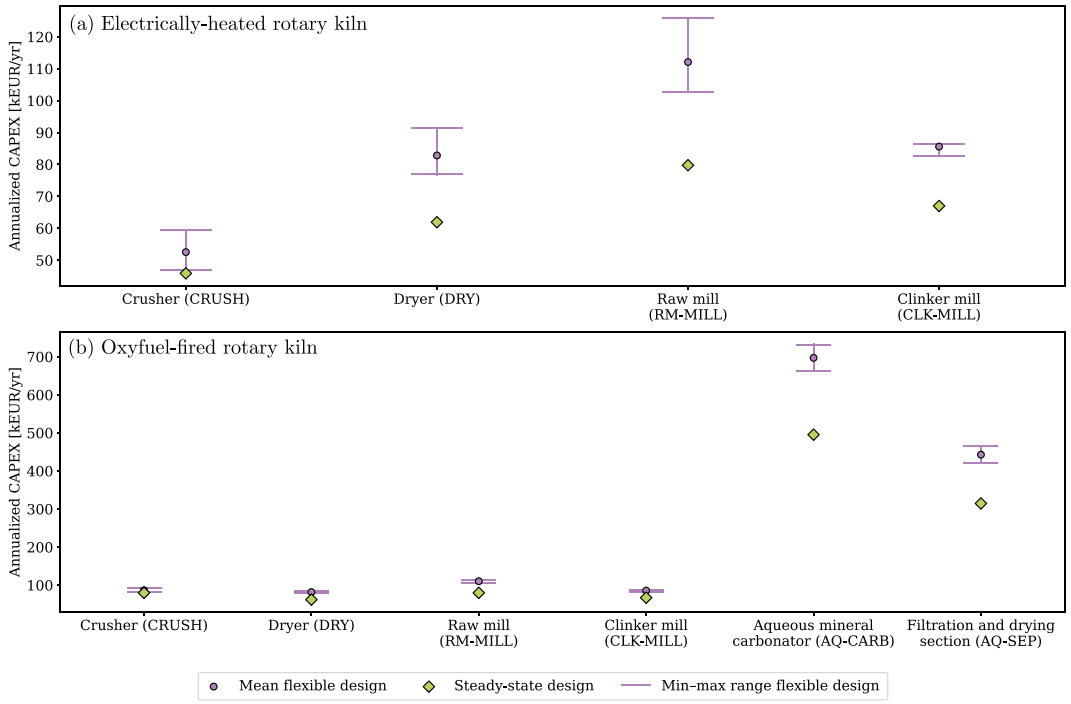

Fig. 10. Annualized capital expenditures (CAPEX) of flexible unit operations compared to the corresponding steady-state configuration for $K = 4, 6, 8, 10, 12, 14, 16, 18,$ and 20 for (a) the electrically-heated rotary kiln-based process and (b) the oxyfuel-fired rotary kiln-based process with biomass. Markers indicate the mean values over the tested temporal aggregations, and bars indicate the min–max range.

Table 4
Storage capacities (in t) for (a) the electrically-heated rotary kiln-based process and (b) the oxyfuel-fired rotary kiln-based process with biomass, for different numbers of clusters.

(a) Electric kiln									
Storage material	Number of clusters								
	4	6	8	10	12	14	16	18	20
Recycled concrete fines	33.3	27.9	18.8	25.0	46.6	49.5	29.1	48.6	54.5
Recycled aggregates[a]	114.3	169.7	224.5	184.8	115.7	50	200.3	90.1	63.3
Raw meal	80	83.5	86.3	88.8	84.9	87.5	90.4	99.2	94.7
Clinker	47.8	50.3	62.4	62.4	62.4	62.4	62.4	65.5	62.4
Ground RC-BCC	47.8	50.3	62.4	62.4	62.4	62.4	62.4	65.5	62.4
(b) Oxyfuel kiln with biomass									
Storage material	Number of clusters								
	4	6	8	10	12	14	16	18	20
Recycled concrete fines	17.6	27.3	24.7	32.2	28.9	28.8	31.4	27.5	26.5
Recycled aggregates[a]	225.4	282.1	360.9	458.2	557.7	409.4	439.7	452.0	463.8
Raw meal	80.7	83.5	83.5	86.4	84.9	87.5	87.5	103.9	100.6
Clinker	47.8	50.3	62.4	62.4	62.4	62.4	62.4	65.5	62.4
Ground RC-BCC	47.8	50.3	62.4	62.4	62.4	62.4	62.4	65.5	62.4
Carbonated aggregates[a]	20.5	17.1	20.5	24.0	27.4	27.4	24.0	31.7	35.6
Captured CO_2	29.2	23.1	24.7	32.6	37.7	38.6	35.1	40.0	41.2

[a] Stored in open stockpiles.

of 50% of RC-BCC, the electrically-heated rotary kiln configuration achieves GWI reductions of 27.1% and 46.5% under high- and low-GWI electricity mixes, respectively. Similarly, the oxyfuel-fired rotary kiln with biomass as fuel configuration achieves GWI reductions of 49.2% (high-GWI electricity mix) and 65.2% (low-GWI electricity mix). If higher RC-BCC substitution levels in the concrete formulation are technically feasible, very low or even negative GWI values could be achieved due to the storage of biogenic CO_2 in the carbonated aggregates. These findings highlight the potential of recycled cementitious materials as enablers of greenhouse gas (GHG) mitigation and material circularity in cement and concrete production. However, achieving drastic GWI reductions would require sufficient amounts of biomass supply and access to a low-carbon electricity mix.

Electricity cost savings and load shifting potential are obtained by flexible operation; however, the overall reduction in total annualized cost (TAC) is marginal. For instance, although the oxyfuel-fired rotary kiln exhibits moderate electricity cost savings of 13.4–18.2% and shifts 25.0–30.6% (10.3–12.6 GWh) of its annual electricity demand, the resulting reduction in TAC is very low (0.09–0.33%). This reflects a trade-off between capital costs and operational costs, i.e., enabling flexibility through the implementation of storage units and equipment oversizing unlocks electricity savings but increases capital investment. Given that these TAC reductions are extremely small, they may be outweighed by model uncertainties, suggesting that the economic benefits of flexibility may remain limited in practice. Moreover, the achievable load shifting potential may be lower due to operational constraints not

implemented in this study, such as ramping limits or start-up energy requirements.

Despite the limitations, the results point to several research directions. First, more detailed demand response models, capable of explicitly representing industrial operational constraints could strengthen the assessment of flexibility. Second, considering longer scheduling horizons, such as weeks instead of days, could provide greater demand response potential. Finally, integrating additional electricity markets, such as intraday or reserve capacity markets, may improve the economic potential of flexible cement plants.

Overall, the integration of RC-BCC and mineral carbonation represents a promising pathway for the deep decarbonization of cement and concrete production, enabling both substantial GHG reductions and enhanced material circularity. While economic benefits remain modest under current assumptions, further research on model uncertainty and large-scale deployment is essential to assess the industrial applicability of RC-BCC-based technologies.

Nomenclature

Abbreviations

AAC	Autoclaved aerated concrete
AEL	Alkaline electrolyzer
ASU	Air separation unit
CAPEX	Capital expenditures
CCU	Carbon capture and utilization
CCUS	Carbon capture, utilization and storage
CEPCI	Chemical Engineering Plant Cost Index
CPU	Carbon purification unit
DR	Demand response
GHG	Greenhouse gas
gRC-BCC	Ground recycled belite cement clinker
GWI	Global warming impact
LHV	Lower heating value
MC	Mineral carbonation
MILP	Mixed integer linear programming
OPEX	Operating expenditures
PC	Portland cement
PCC	Portland cement clinker
pd-AAC	Post-demolition autoclaved aerated concrete
PEMEL	Proton exchange membrane electrolyzer
rA	Recycled aggregates
RC-BCC	Recycled belite cement clinker
rCF	Recycled concrete fines
SRMs	Secondary raw materials
TAC	Total annualized cost
TRL	Technology readiness level

Greek symbols

α	Scale factor
ΔH	Enthalpy of reaction
ΔT	Temperature difference
Δt	Duration of one time step
η	Efficiency
γ	Project lifetime
ν	Stoichiometric coefficient
ω	Cluster weight
ϕ	Design fraction
σ	Interest rate of investment
ζ	Splitter fraction

Latin symbols

$\mathcal{C}$	Set of components
$\mathcal{C}^{ns}$	Set of non-storage components
c	Heat capacity
CE	CEPCI value
CRF	Capital recovery factor
CS	Carbon credits
CX	Capital costs
D	Size of component
$\mathcal{E}$	Set of electricity-based units
$\mathcal{E}_u$	Set of reactants
$\dot{E}$	Energy flow
EF	Emission factor
$\mathcal{F}_c^{E,in}$	Set of incoming energy flows of component c
$\mathcal{F}_c^{E,out}$	Set of outgoing energy flows of component c
$\mathcal{F}_c^{M,in}$	Set of incoming material flows of component c
$\mathcal{F}_c^{M,out}$	Set of outgoing material flows of component c
$\mathcal{G}_u$	Set of products
GWI	Global warming impact
$\mathcal{H}$	Set of hourly periods within a day
$\mathcal{K}$	Set of typical-day clusters
$\mathcal{L}$	Set of splitters
$\mathcal{M}$	Set of material sources
$\dot{M}$	Material flow
m^{cem}	Mass of cement blend
m^{lime}	Mass of limestone
m^{PC}	Mass of Portland cement
m^{rCF}	Mass of recycled concrete fines
m^{RC-BCC}	Mass of recycled belite cement clinker
m^{rm}	Mass of raw meal
$\mathcal{N}$	Set of sinks
OX	Operating costs
p	Commodity/certificate price
p^{min}	Minimum part-load factor
$\mathcal{Q}$	Set of thermal units
$\mathcal{S}$	Set of commodities
$\dot{S}$	Energy or material flow from source or to sink
SOC	State of charge
$\mathcal{T}$	Set of time steps
T	Maintenance cost factor
TAC	Total annualized cost
$\mathcal{U}$	Set of conversion units
$\mathcal{W}$	Set of storage units
w	Molecular weight
$\mathcal{X}$	Set of mixers
x	Decision to install a component
y	Decision to operate a component

Subscripts

batch-mix	Batching and mixing section
bCO_2	Biogenic CO_2
bio	Biomass
c	Component
cem	Cement blend
e	Reactant
el	Electric
g	Product
h	Hourly period
heat	Thermal heat
i	Incoming energy or material flow index
j	Outgoing energy or material flow index
k	Typical-day cluster
l	Splitter
lime	Limestone
m	Mass source
n	Sink
NG	Natural gas
PC	Portland cement
q	Thermal unit
RC-BCC	Recycled belite cement clinker

rCF	Recycled concrete fines
rm	Raw meal
rm-mill	Raw mill
s	Commodity
u	Conversion unit
w	Storage unit
x	Mixer
Superscripts	
cem	Cement
dir	Direct
fix	Fixed
fos	Fossil
in	Input
ind	Indirect
lime	Limestone
max	Maximum
min	Minimum
nom	Nominal
ope	Operating
out	Output
PC	Portland cement
RC-BCC	Recycled belite cement clinker
rCF	Recycled concrete fines
ref	Reference
rm	Raw meal
util	Utilized
var	Variable

CRediT authorship contribution statement

Ariana Y. Ojeda-Paredes: Writing – original draft, Visualization, Software, Methodology, Investigation, Formal analysis, Data curation, Conceptualization. **Gourisankar Sandaka:** Writing – review & editing, Methodology, Conceptualization. **Günter Beuchle:** Writing – review & editing, Methodology, Conceptualization. **Peter Stemmermann:** Writing – review & editing, Methodology, Funding acquisition, Conceptualization. **Dieter Stapf:** Writing – review & editing, Funding acquisition. **Alexander Mitsos:** Writing – review & editing, Supervision, Funding acquisition. **Manuel Dahmen:** Writing – review & editing, Supervision, Methodology, Funding acquisition, Conceptualization.

Declaration of competing interest

The authors declare the following financial interests/personal relationships which may be considered as potential competing interests: The authors report that financial support was provided by the Helmholtz Association of German Research Centers. Given his role as editor of Computers and Chemical Engineering, Alexander Mitsos had no involvement in the peer review of this article and had no access to information regarding its peer review. Full responsibility for the editorial process for this article was delegated to another journal editor. If there are other authors, they declare that they have no known competing financial interests or personal relationships that could have appeared to influence the work reported in this paper.

Acknowledgments

This work was funded by the Helmholtz Association of German Research Centers through program-oriented funding and the Innovation Pool projects “Energiewende und Kreislaufwirtschaft” (energy transition and circular economy) and “Industrielle Transformation 2050” (industrial transformation 2050).

Appendix A. Supplementary data

Supplementary material related to this article can be found online at https://doi.org/10.1016/j.compchemeng.2026.109750.

Data availability

Data sharing not applicable to this article.

References

Abbasi, T., Abbasi, S., 2010. Biomass energy and the environmental impacts associated with its production and utilization. Renew. Sustain. Energy Rev. 14 (3), 919–937.

Assunção, R., Ajeeb, W., Eckl, F., Gomes, D.M., Neto, R.C., 2025. Decentralized hydrogen-oxygen co-production via electrolysis for large hospitals with integrated hydrogen refueling station. Int. J. Hydrog. Energy 103, 87–98.

Atmaca, A., Atmaca, N., 2016. Determination of correlation between specific energy consumption and vibration of a raw mill in cement industry. Anadolu Univ. J. Sci. Technol. A - Appl. Sci. Eng. 17 (1), 209–219.

Back, J., Zevenhoven, R., Fagerlund, J., Sorjonen-Ward, P., 2022. Mineral carbonation using mine tailings-A strategic overview of potential and opportunities. In: Proceedings of the 16th Greenhouse Gas Control Technologies Conference. GHGT-16, pp. 23–24.

Baena-Moreno, F.M., Rodríguez-Galán, M., Vega, F., Alonso-Fariñas, B., Arenas, L.F.V., Navarrete, B., 2019. Carbon capture and utilization technologies: a literature review and recent advances. Energy Sources, Part A: Recovery Util. Environ. Eff. 41 (12), 1403–1433.

Barbhuiya, S., Kanavaris, F., Das, B.B., Idrees, M., 2024. Decarbonising cement and concrete production: Strategies, challenges and pathways for sustainable development. J. Build. Eng. 86, 108861.

Bhandari, R., Trudewind, C.A., Zapp, P., 2014. Life cycle assessment of hydrogen production via electrolysis – a review. J. Clean. Prod. 85, 151–163, Special Volume: Making Progress Towards More Sustainable Societies through Lean and Green Initiatives.

Bhatnagar, S., Popuri, A.K., 2024. Overview of energy consumption and attributes of grinding technologies in Indian cement industry. ZKG Int. (6), 1–10. http://dx.doi.org/10.32604/zkg.2024.06.02.

Bolte, G., Zajac, M., Skocek, J., Ben Haha, M., 2019. Development of composite cements characterized by low environmental footprint. J. Clean. Prod. 226, 503–514.

Bremen, A.M., Strunge, T., Ostovari, H., Spütz, H., Mhamdi, A., Renforth, P., van der Spek, M., Bardow, A., Mitsos, A., 2022. Direct olivine carbonation: Optimal process design for a low-emission and cost-efficient cement production. Ind. Eng. Chem. Res. 61 (35), 13177–13190.

Buhre, B., Elliott, L., Sheng, C., Gupta, R., Wall, T., 2005. Oxy-fuel combustion technology for coal-fired power generation. Prog. Energy Combust. Sci. 31 (4), 283–307.

Bundesministerium für Wohnen, Stadtentwicklung und Bauwesen, 2024. Ready-mix concrete C25/30 (EN 206) – generic [dataset, version 20.24.070]. ÖKOBAUDAT – Sustainable Construction Information Portal. URL: https://oekobaudat.de/OEKOBAU.DAT/datasetdetail/process.xhtml?uuid=a71e60a5-b64b-4715-ae8a-c8c8819149d2&version=20.24.070&stock=OBD_2024_I&lang=en. (Accessed 19 June 2025).

Bundesnetzagentur and Bundeskartellamt, 2024. Monitoringbericht 2024. Report. Bundesnetzagentur und Bundeskartellamt. https://data.bundesnetzagentur.de/Bundesnetzagentur/SharedDocs/Mediathek/Monitoringberichte/MonitoringberichtEnergie2024.pdf (Accessed 25 June 2025).

Bundesnetzagentur|SMARD.de, 2024. SMARD Strommarktdaten. URL: https://www.smard.de/. (Accessed 25 June 2025).

Buttler, A., Spliethoff, H., 2018. Current status of water electrolysis for energy storage, grid balancing and sector coupling via power-to-gas and power-to-liquids: A review. Renew. Sustain. Energy Rev. 82, 2440–2454.

C.A.R.M.E.N. e.V., 2024. Marktpreise Hackschnitzel. https://www.carmen-ev.de/ (Accessed 25 June 2025).

Castro, P.M., Sun, L., Harjunkoski, I., 2013. Resource–task network formulations for industrial demand side management of a steel plant. Ind. Eng. Chem. Res. 52 (36), 13046–13058.

CemNet, 2025. Cement industry turns to concrete recycling to drive circular economy. https://www.cemnet.com/News/story/179975/cement-industry-turns-to-concrete-recycling-to-drive-circular-economy (Accessed 02 February 2026).

Chakraborty, S., Jo, B.W., 2018. 3 - aqueous-based carbon dioxide sequestration. In: Pacheco-Torgal, F., Shi, C., Sanchez, A.P. (Eds.), Carbon Dioxide Sequestration in Cementitious Construction Materials. In: Woodhead Publishing Series in Civil and Structural Engineering, Woodhead Publishing, pp. 39–64.

Chardonnet, C., Giordano, V., Rapoport, S., De Vos, L., Genoese, F., Roig, G., Bart, F., Lanoix, J., Vanhoudt, W., De Lacroix, T., Ha, T., Van Genabet, B., 2017. Study on early business cases for H_2 in energy storage and more broadly power to H_2 applications. Report, Fuel Cells and Hydrogen 2 Joint Undertaking (FCH 2 JU). URL: https://www.fch.europa.eu/sites/default/files/P2H_Full_Study_FCHJU.pdf. (Accessed 25 June 2025).

Chart Industries, 2021. Carbon dioxide storage tank technical manual (Rev. I). Technical manual, form 11650869 Rev. I, Chart Industries Inc. https://files.chartindustries.com/11650869_Carbon_Dioxide_Storage_Tank_Tech_Manual_Rev_I_ws.pdf (Accessed 02 October 2025).

CLIMIT Programme, 2020. Combined calcination and CO_2 capture in cement clinker production by use of CO_2-neutral electrical energy – phase 2 (ELSE 2). https://climit.no/en/project/combined-calcination-and-co2-capture-in-cement-clinker-production-by-use-of-co2-neutral-electrical-energy-phase-2-else-2/. (Accessed 19 June 2025). Project Report, CLIMIT CO_2 Management Programme.

Co–Reactive, 2024. About us: Carbon mineralization technology. https://www.co-reactive.com/#about-us (Accessed 04 March 2026).

Cuéllar-Franca, R.M., Azapagic, A., 2015. Carbon capture, storage and utilisation technologies: A critical analysis and comparison of their life cycle environmental impacts. J. CO2 Util. 9, 82–102.

Deolalkar, S.P., 2009. Handbook for Designing Cement Plants. BS Publications, Hyderabad, India.

Ditaranto, M., Bakken, J., 2019. Study of a full scale oxy-fuel cement rotary kiln. Int. J. Greenh. Gas Control. 83, 166–175.

ECRA, 2009. ECRA CCS Project—Report about Phase II. Report TR-ECRA-106/2009. European Cement Research Academy GmbH. https://ecra-online.org/search/?q=technical+report+phase+II (Accessed 01 August 2024).

EEX, 2024. Emission spot primary market auction report 2024. Report. European Energy Exchange. https://www.eex.com/en/market-data/environmental-markets/eua-primary-auction-spot-download (Accessed 02 October 2025).

El-Emam, R.S., Gabriel, K.S., 2021. Synergizing hydrogen and cement industries for Canada's climate plan – case study. Energy Sources, Part A: Recovery Util. Environ. Eff. 43 (23), 3151–3165.

Estelmann, S., Dietrich, R.-U., Seitz, A., 2018. Flexibilitätsoptionen in der Grundstoffindustrie Methodik | Potenziale | Hemmnisse. https://elib.dlr.de/119879/ (Accessed 02 October 2025).

Faria, D.G., Carvalho, M.M., Neto, M.R., de Paula, E.C., Cardoso, M., Vakkilainen, E.K., 2022. Integrating oxy-fuel combustion and power-to-gas in the cement industry: A process modeling and simulation study. Int. J. Greenh. Gas Control. 114, 103602.

Floudas, C.A., Lin, X., 2004. Continuous-time versus discrete-time approaches for scheduling of chemical processes: a review. Comput. Chem. Eng. 28, 2109–2129.

Fraunhofer ISI, 2024. Direct electrification of industrial process heat. An assessment of technologies, potentials and future prospects for the EU. Study on behalf of Agora Industry. https://www.agora-industry.org/publications/direct-electrification-of-industrial-process-heat (Accessed 16 September 2025).

Gardarsdottir, S.O., De Lena, E., Romano, M., Roussanaly, S., Voldsund, M., Pérez-Calvo, J.-F., Berstad, D., Fu, C., Anantharaman, R., Sutter, D., Gazzani, M., Mazzotti, M., Cinti, G., 2019. Comparison of technologies for CO_2 capture from cement production— Part 2: Cost analysis. Energies 12 (3), 542.

Gartner, E., Sui, T., 2018. Alternative cement clinkers. Cem. Concr. Res. 114, 27–39.

Genç, Ö., 2016. Energy-efficient technologies in cement grinding. In: Yilmaz, S., Ozmen, H.B. (Eds.), High Performance Concrete Technology and Applications. IntechOpen, London, Chapter 6.

Germscheid, S.H., Röben, F.T., Sun, H., Bardow, A., Mitsos, A., Dahmen, M., 2023. Demand response scheduling of copper production under short-term electricity price uncertainty. Comput. Chem. Eng. 178, 108394.

Global CCS Institute, 2018. Callide Oxyfuel Project – Final Results Public Report. https://letaustralia.com.au/wp-content/uploads/cop-final-results-public-report-march-2018-1.pdf (Accessed 02 October 2025).

Glover, F., 1975. Improved linear integer programming formulations of nonlinear integer problems. Manag. Sci. 22 (4), 455–460.

Golmohamadi, H., 2022. Demand-side management in industrial sector: A review of heavy industries. Renew. Sustain. Energy Rev. 156, 111963.

Grammelis, P., Margaritis, N., Karampinis, E., 2016. Solid Fuel Types for Energy Generation: Coal and Fossil Carbon-Derivative Solid Fuels. Woodhead Publishing, Boston, pp. 29–58.

Griffiths, S., Sovacool, B.K., Furszyfer Del Rio, D.D., Foley, A.M., Bazilian, M.D., Kim, J., Uratani, J.M., 2023. Decarbonizing the cement and concrete industry: A systematic review of socio-technical systems, technological innovations, and policy options. Renew. Sustain. Energy Rev. 180, 113291.

Gurobi Optimization, LLC, 2020. Gurobi optimizer version 9.5.1. http://www.gurobi.com (Accessed 01 June 2025).

Helin, K., Käki, A., Zakeri, B., Lahdelma, R., Syri, S., 2017. Economic potential of industrial demand side management in pulp and paper industry. Energy 141, 1681–1694.

Hills, T., Leeson, D., Florin, N., Fennell, P., 2016. Carbon capture in the cement industry: Technologies, progress, and retrofitting. Environ. Sci. Technol. 50, 368–377.

Hunsinger, H., Beuchle, G., Stemmermann, P., Schweike, U., Warzycha, K., Garbev, K., 2014. Verfahren zur herstellung von dicalciumsilikat. Karlsruher Institut für Technologie. WO 2014/019656 A1.

Icha, P., Lauf, T., 2025. Entwicklung der spezifischen Treibhausgas-Emissionen des deutschen Strommix in den Jahren 1990 - 2024. Report Climate Change 15/2022. Umweltbundesamt. https://www.umweltbundesamt.de/publikationen/entwicklung-der-spezifischen-treibhausgas-11 (Accessed 25 June 2025).

Iizuka, A., Fujii, M., Yamasaki, A., Yanagisawa, Y., 2004. Development of a new CO_2 sequestration process utilizing the carbonation of waste cement. Ind. Eng. Chem. Res. 43 (24), 7880–7887.

Information und Technik Nordrhein-Westfalen (IT.NRW), 2024. NRW-industrie: Gewinnung von kies, sand und ton 2024 auf dem niedrigsten stand seit 2014. URL: https://www.it.nrw/nrw-industrie-gewinnung-von-kies-sand-und-ton-2024-auf-dem-niedrigsten-stand-seit-2014-127406. (Accessed 25 June 2025).

International Energy Agency-Greenhouse Gas R&D Programme (IEA-GHG), 2013. Deployment of CCS in the cement industry. Report 2013/19. https://ieaghg.org/docs/General_Docs/Reports/2013-19.pdf (Accessed 10 October 2024).

International Energy Agency (IEA), 2018. Technology roadmap - low-carbon transition in the cement industry. Report. https://www.iea.org/reports/technology-roadmap-low-carbon-transition-in-the-cement-industry (Accessed 01 August 2024).

International Energy Agency (IEA), 2021. Net Zero by 2050: A Roadmap for the global energy sector. Report. https://www.iea.org/reports/net-zero-by-2050 (Accessed 28 August 2025).

International Energy Agency (IEA), 2022. Norway 2022. Energy policy review. Report. https://www.iea.org/reports/norway-2022/executive-summary (Accessed 28 August 2025).

International Energy Agency (IEA) Bioenergy, 2008. The availability of biomass resources for energy: Summary and conclusions – ExCo58 Workshop. https://www.ieabioenergy.com/wp-content/uploads/2013/10/The-Availability-of-Biomass-Resources-for-Energy-Sumamry-and-Conclusions.pdf (Accessed 23 April 2026).

International Energy Agency (IEA) Bioenergy, 2021. Deployment of bio-CCS in the cement sector: an overview of technology options and policy tools. Report. https://www.ieabioenergy.com/wp-content/uploads/2022/03/bio-CCS-in-the-cement-sector.pdf (Accessed 23 April 2026).

Ishak, S.A., Hashim, H., 2015. Low carbon measures for cement plant - A review. J. Clean. Prod. 103, 260–274.

Jackson, S., Brodal, E., 2019. Optimization of the energy consumption of a carbon capture and sequestration related carbon dioxide compression processes. Energies 12 (9), 1603.

Juangsa, F.B., Cezeliano, A.S., Darmanto, P.S., Aziz, M., 2022. Thermodynamic analysis of hydrogen utilization as alternative fuel in cement production. South Afr. J. Chem. Eng. 42, 23–31.

Kendall, A., Kesler, S.E., Keoleian, G.A., 2010. Megaquarry versus decentralized mineral production: network analysis of cement production in the Great Lakes region, USA. J. Transp. Geogr. 18 (2), 322–330.

Kermeli, K., Worrell, E., Masanet, E., 2011. Energy efficiency improvement and cost saving opportunities for the concrete industry: An ENERGY STAR® guide for energy and plant managers. https://www.osti.gov/servlets/purl/1062106 (Accessed 19 June 2025).

Langiu, M., Shu, D.Y., Baader, F.J., Hering, D., Bau, U., Xhonneux, A., Müller, D., Bardow, A., Mitsos, A., Dahmen, M., 2021. COMANDO: A next-generation open-source framework for energy systems optimization. Comput. Chem. Eng. 152, 107366.

Lechtenböhmer, S., Nilsson, L.J., Åhman, M., Schneider, C., 2016. Decarbonising the energy intensive basic materials industry through electrification – Implications for future EU electricity demand. Energy 115, 1623–1631, Sustainable Development of Energy, Water and Environment Systems.

LEILAC2 Project, 2023. A techno-economic analysis of the leilac technology at full commercial scale. https://www.leilac.com/wp-content/uploads/2023/10/2023-10-15-Techno-Economic-Analysis-of-Leilac-Technology-at-Full-Commercial-Scale-EC-Deliverable-PDF-Version.pdf (Accessed 19 June 2025).

Li, S., Jiang, N., Zhou, K., Jiao, X., 2014. Rotary kiln for producing lime through calcination by using electric heating device. Chinese patent CN102627416B. https://patents.google.com/patent/CN102627416B/en (Accessed 02 February 2026).

Luo, J., Moncada, J., Ramirez, A., 2022. Development of a conceptual framework for evaluating the flexibility of future chemical processes. Ind. Eng. Chem. Res. 61 (9), 3219–3232.

MacQueen, J., 1967. Some methods for classification and analysis of multivariate observations. In: Proceedings of the Fifth Berkeley Symposium on Mathematical Statistics and Probability. Vol. 1, University of California Press, Berkeley, CA, USA, pp. 281–297.

Madeddu, S., Ueckerdt, F., Pehl, M., Peterseim, J., Lord, M., Kumar, K.A., Krüger, C., Luderer, G., 2020. The CO_2 reduction potential for the European industry via direct electrification of heat supply (power-to-heat). Environ. Res. Lett. 15 (12), 124004.

Marmier, A., 2023. Decarbonisation options for the cement industry. JRC131246. Publications Office of the European Union. https://publications.jrc.ec.europa.eu/repository/handle/JRC131246 (Accessed 19 June 2025).

Marsh, A.T., Velenturf, A.P., Bernal, S.A., 2022. Circular economy strategies for concrete: implementation and integration. J. Clean. Prod. 362, 132486.

Material Economics, 2019. Industrial transformation 2050: Pathways to net-zero emissions from EU heavy industry. https://materialeconomics.com/node/13 (Accessed 19 June 2025).

Mavrotas, G., 2009. Effective implementation of the ϵ-constraint method in multi-objective mathematical programming problems. Appl. Math. Comput. 213 (2), 455–465.

Meng, R., Zhao, Q., Wu, M., Long, Q., Zhou, M., 2021. A survey and analysis on electricity consumption of raw material mill system in China cement industry between 2014 and 2019. Sustainability 13 (3), 1126.

Metz, B., Davidson, O., De Coninck, H., Loos, M., Meyer, L., 2005. Carbon Dioxide Capture and Storage: Special Report of the Intergovernmental Panel on Climate Change. Cambridge University Press.

Mignogna, D., Szabó, M., Ceci, P., Avino, P., 2024. Biomass energy and biofuels: Perspective, potentials, and challenges in the energy transition. Sustainability 16 (16), 7036.

Miller, B.G., 2011. 10 - CO2 capture and storage. In: Miller, B.G. (Ed.), Clean Coal Engineering Technology. Butterworth-Heinemann, Boston, pp. 483–511.

Mitsos, A., Asprion, N., Floudas, C.A., Bortz, M., Baldea, M., Bonvin, D., Caspari, A., Schäfer, P., 2018. Challenges in process optimization for new feedstocks and energy sources. Comput. Chem. Eng. 113, 209–221.

Mossie, A.T., Khatiwada, D., Palm, B., Bekele, G., 2025. Energy demand flexibility potential in cement industries: How does it contribute to energy supply security and environmental sustainability? Appl. Energy 377, 124608.

Nhuchhen, D.R., Sit, S.P., Layzell, D.B., 2021. Alternative fuels co-fired with natural gas in the pre-calciner of a cement plant: Energy and material flows. Fuel 295, 120544.

Noche, B., Elhasia, T., 2013. Approach to innovative supply chain strategies in cement industry; analysis and model simulation. Procedia - Soc. Behav. Sci. 75, 359–369, The Second International Conference on Leadership, Technology and Innovation Management (2012).

Nussbaumer, T., 2003. Combustion and co-combustion of biomass: Fundamentals, technologies, and primary measures for emission reduction. Energy & Fuels 17 (6), 1510–1521.

Ojeda-Paredes, A.Y., Mitsos, A., Dahmen, M., 2025. Retrofitting ordinary Portland cement production for reduced greenhouse gas emissions. Comput. Chem. Eng. 201, 109200.

OneStone Consulting, 2024. Germany's cement prices slightly decreased. https://ccf2up.com/germanys-cement-prices-slightly-decreased/ (Accessed 25 June 2025).

Ozturk, M., Dincer, I., 2022. Utilization of waste heat from cement plant to generate hydrogen and blend it with natural gas. Int. J. Hydrog. Energy 47 (48), 20695–20704.

Paulus, M., Borggrefe, F., 2011. The potential of demand-side management in energy-intensive industries for electricity markets in Germany. Appl. Energy 88 (2), 432–441, The 5th Dubrovnik Conference on Sustainable Development of Energy, Water and Environment Systems, held in Dubrovnik September/October 2009.

Pedraza, J., Zimmermann, A., Tobon, J., Schomäcker, R., Rojas, N., 2021. On the road to net zero-emission cement: Integrated assessment of mineral carbonation of cement kiln dust. Chem. Eng. J. 408, 127346.

Pedregosa, F., Varoquaux, G., Gramfort, A., Michel, V., Thirion, B., Grisel, O., Blondel, M., Prettenhofer, P., Weiss, R., Dubourg, V., Vanderplas, J., Passos, A., Cournapeau, D., Brucher, M., Perrot, M., Duchesnay, É., 2011. Scikit-learn: Machine learning in Python. J. Mach. Learn. Res. 12, 2825–2830.

Pisciotta, M., Pilorgé, H., Feldmann, J., Jacobson, R., Davids, J., Swett, S., Sasso, Z., Wilcox, J., 2022. Current state of industrial heating and opportunities for decarbonization. Prog. Energy Combust. Sci. 91, 100982.

Plaza, M.G., Martínez, S., Rubiera, F., 2020. CO_2 Capture, use, and storage in the cement industry: State of the art and expectations. Energies 13 (21), 5692.

Quevedo Parra, S., Romano, M.C., 2023. Decarbonization of cement production by electrification. J. Clean. Prod. 425, 138913.

Röben, F.T., Liu, D., Reuter, M.A., Dahmen, M., Bardow, A., 2022. The demand response potential in copper production. J. Clean. Prod. 362, 132221.

Röben, F.T., Schöne, N., Bau, U., Reuter, M.A., Dahmen, M., Bardow, A., 2021. Decarbonizing copper production by power-to-hydrogen: A techno-economic analysis. J. Clean. Prod. 306, 127191.

Rodríguez, N., Murillo, R., Abanades, J.C., 2012. CO_2 capture from cement plants using oxyfired precalcination and/or calcium looping. Environ. Sci. Technol. 46 (4), 2460–2466.

Rojas-Innocenti, S., Baeyens, E., Martín-Crespo, A., Saludes-Rodil, S., Frechoso, F., 2024. Enhancing industrial flexibility and market participation in cement manufacturing through optimized production scheduling. arXiv preprint arXiv:2403.06573 Preprint.

Sabbah, A., Zhutovsky, S., 2022. Effect of sulfate content and synthesis conditions on phase composition of belite-ye'elimite-ferrite (BYF) clinker. Cem. Concr. Res. 155, 106745.

Sanna, A., Hall, M.R., Maroto-Valer, M., 2012. Post-processing pathways in carbon capture and storage by mineral carbonation (CCSM) towards the introduction of carbon neutral materials. Energy Env. Sci. 5, 7781–7796.

Sanna, A., Uibu, M., Caramanna, G., Kuusik, R., Maroto-Valer, M.M., 2014. A review of mineral carbonation technologies to sequester CO2. Chem. Soc. Rev. 43, 8049–8080.

Schäfer, P., Daun, T.M., Mitsos, A., 2020. Do investments in flexibility enhance sustainability? A simulative study considering the German electricity sector. AIChE J. 66 (11), e17010.

Schlögl, R., Abanades, C., Aresta, M., Azapagic, A., Blekkan, E.A., Cantat, T., Centi, G., Duic, N., El Khamlichi, A., Hutchings, G., et al., 2018. Novel Carbon Capture and Utilisation Technologies: Research and Climate Aspects. Technical Report, SAPEA – Science Advice for Policy by European Academies, Berlin, URL: https://pure.mpg.de/rest/items/item_2638453/component/file_2638452/content. (Accessed 25 June 2025).

Schoon, J., De Buysser, K., Van Driessche, I., De Belie, N., 2013. Feasibility study on the use of cellular concrete as alternative raw material for Portland clinker production. Constr. Build. Mater. 48, 725–733.

Schorcht, F., Kourti, I., Scalet, B.M., Roudier, S., Sancho, L.D., 2013. Best available techniques BAT reference document for the production of cement, lime and magnesium oxide. Report. Industrial emissions directive 2010/75/EU European commission. https://eippcb.jrc.ec.europa.eu/reference/production-cement-lime-and-magnesium-oxide (Accessed 01 August 2024).

Siddiquee, S.M.S., Howard, B., Bruton, K., Brem, A., O'Sullivan, D.T.J., 2021. Progress in demand response and it's industrial applications. Front. Energy Res. Volume 9 - 2021.

Smith, I., 2003. Co-utilisation of Coal and Other Fuels in Cement Kilns. Technical Report, IEA Clean Coal Centre, London, United Kingdom, URL: https://www.osti.gov/etdeweb/biblio/20390254. (Accessed 25 June 2025).

Smith, R., 2016. Chemical Process Design and Integration, Second ed. Wiley, Chichester, West Sussex, United Kingdom, 2016.

Song, X., Xiaoyu, C., Lin, Q., Yanna, L., 2019. A review of mineral carbonation from industrial waste. IOP Conf. Ser.: Earth Environ. Sci. 401 (1), 012008.

Spath, P.L., Mann, M.K., 2004. Life cycle assessment of renewable hydrogen production via wind/electrolysis. National Renewable Energy Laboratory (NREL). https://www.nrel.gov/docs/fy04osti/35404.pdf (Accessed 05 December 2025).

Statista, 2024. Produktion der transportbetonindustrie in Deutschland nach betonsorten im jahr 2023. https://de.statista.com/statistik/daten/studie/167020/umfrage/produktion-der-transportbetonindustrie-nach-betonsorten/ (Accessed 19 June 2025).

Steins, J.J., Volk, R., Schultmann, F., 2022. Post-demolition autoclaved aerated concrete: Recycling options and volume prediction in Europe. In: Ecocity World Summit 2021- Conference Proceedings. pp. 259–267.

Stemmermann, P., Ullrich, A., Beuchle, G., Garbev, K., Schweike, U., 2022. Belite cement clinker from autoclaved aerated concrete waste – A contribution towards CO_2-reduced circular building materials. Ce/Papers 5 (5), 17–26.

Stemmermann, P., Volk, R., Steins, J., Beuchle, G., 2024. Recycling belite cement clinker from post-demolition autoclaved aerated concrete – assessing a new process. Resour. Conserv. Recycl. 203, 107404.

Summerbell, D.L., Khripko, D., Barlow, C., Hesselbach, J., 2017. Cost and carbon reductions from industrial demand-side management: Study of potential savings at a cement plant. Appl. Energy 197, 100–113.

Swaney, R.E., Grossmann, I.E., 1985. An index for operational flexibility in chemical process design. Part I: Formulation and theory. AIChE J. 31 (4), 621–630.

Tan, B., Okoronkwo, M.U., Kumar, A., Ma, H., 2020. Durability of calcium sulfoaluminate cement concrete. J. Zhejiang Univ.-Sci. A 21 (2), 118–128.

Thiran, P., Jeanmart, H., Contino, F., 2023. Validation of a method to select a priori the number of typical days for energy system optimisation models. Energies 16 (6), 2772.

Thonemann, N., Zacharopoulos, L., Fromme, F., Nühlen, J., 2022. Environmental impacts of carbon capture and utilization by mineral carbonation: A systematic literature review and meta life cycle assessment. J. Clean. Prod. 332, 130067.

Tokheim, L.-A., Mathisen, A., Øi, L.E., Jayarathna, C., Eldrup, N., Gautestad, T., 2019. Combined calcination and CO_2 capture in cement clinker production by use of electrical energy. In: Proceedings of the 10th International Trondheim CCS Conference. TCCS-10, Trondheim, Norway, p. 17, Presented at TCCS-10, 17–19 June 2019.

Tsupari, E., Korpijärvi, K., Kauppinen, J., Pikkarainen, T., Leino, T., Simell, P., Lappalainen, M., Winberg, I., Katajisto, O., Mäkikouri, S., 2022. Reducing the climate impacts of industry through carbon-neutral energy and the circular economy – decarbonate. https://www.decarbonate.fi/wp-content/uploads/2022/06/Decarbonate_Final_report.pdf (Accessed 19 June 2025).

van Leeuwen, C., Zauner, A., 2018. Innovative Large-Scale Energy Storage Technologies and Power-To-Gas Concepts After Optimisation: report on the Costs Involved with PtG Technologies and Their Potentials Across the EU. D8.3. Technical Report, European Commission CORDIS, URL: https://cordis.europa.eu/project/id/691797/results. (Accessed 25 June 2025).

Vanderzee, S., Zeman, F., 2018. Recovery and carbonation of 100% of calcium in waste concrete fines: Experimental results. J. Clean. Prod. 174, 718–727.

Varnier, L., d'Amore, F., Clausen, K., Melitos, G., de Groot, B., Bezzo, F., 2025. Combined electrification and carbon capture for low-carbon cement: Techno-economic assessment of different designs. J. Clean. Prod. 498, 145029.

Verein Deutscher Zementwerke e.V. (VDZ), 2022. Umwelt-Produktdeklaration nach ISO 14025 und EN 15804+A2 – Portlandzement (CEM I). EPD-VDZ-20220153-IAG1-DE, Institut Bauen und Umwelt e.V. URL: https://www.beton.org/fileadmin/beton-org/media/Dokumente/PDF/Wissen/Beton-Bautechnik/Nachhaltigkeit/2022-06-08-EPD-CEM_I-D.pdf. (Accessed 25 June 2025).

Vielma, J.P., Ahmed, S., Nemhauser, G., 2010. Mixed-integer models for nonseparable piecewise-linear optimization: Unifying framework and extensions. Oper. Res. 58 (2), 303–315.

Voldsund, M., Anantharaman, R., Berstad, D., Cinti, G., De Lena, E., Fu, S., Jamali, A., Pérez-Calvo, J., Romano, M., Roussanaly, S., Ruppert, J., Stallmann, O., Sutter, D., 2018. CEMCAP comparative techno-economic analysis of CO_2 capture in cement plants (D4.6).

Voldsund, M., Gardarsdottir, S.O., Lena, E.D., Pérez-Calvo, J.F., Jamali, A., Berstad, D., Fu, C., Romano, M., Roussanaly, S., Anantharaman, R., Hoppe, H., Sutter, D., Mazzotti, M., Gazzani, M., Cinti, G., Jordal, K., 2019. Comparison of technologies for CO_2 capture from cement production— Part 1: Technical evaluation. Energies 12.

Voll, P., Klaffke, C., Hennen, M., Bardow, A., 2013. Automated superstructure-based synthesis and optimization of distributed energy supply systems. Energy 50, 374–388.

Walker, N., Bazilian, M., Buckley, P., 2009. Possibilities of reducing CO_2 emissions from energy-intensive industries by the increased use of forest-derived fuels in Ireland. Biomass Bioenergy 33 (9), 1229–1238.

Yang, F., Meerman, H., Zhang, Z., Jiang, J., Faaij, A., 2022. Integral techno-economic comparison and greenhouse gas balances of different production routes of aromatics from biomass with CO_2 capture. J. Clean. Prod. 372, 133727.

Zajac, M., Skocek, J., Ben Haha, M., Deja, J., 2022. CO_2 mineralization methods in cement and concrete industry. Energies 15 (10), 3597.

Zajac, M., Skocek, J., Skibsted, J., Ben Haha, M., 2021. CO_2 mineralization of demolished concrete wastes into a supplementary cementitious material – a new CCU approach for the cement industry. RILEM Tech. Lett. 6, 53–60.

Zhang, Q., Grossmann, I.E., 2016. Planning and scheduling for industrial demand side management: Advances and challenges. In: Martín, M. (Ed.), Alternative Energy Sources and Technologies. Springer International Publishing, pp. 383–414.

Zhu, X., Zhang, Y., Liu, Z., Qiao, H., Ye, F., Lei, Z., 2023. Research on carbon emission reduction of manufactured sand concrete based on compressive strength. Constr. Build. Mater. 403, 133101.